

The Influence of Air–Sea Roughness, Sea Spray, and Storm Translation Speed on Waves in North Atlantic Storms

WEIQING ZHANG

Environment Canada, Downsview, Ontario, Canada

WILLIAM PERRIE

Fisheries & Oceans Canada, Bedford Institute of Oceanography, Dartmouth, Nova Scotia, Canada

(Manuscript received 1 November 2006, in final form 20 August 2007)

ABSTRACT

A coupled atmosphere–wave–sea spray model system is used to evaluate the impact of sea spray and wave drag on storm-generated waves, their height variations, and directional wave spectra in relation to the storm location and translation speed. Results suggest that the *decrease* or *increase* of significant wave height due to spray and wave drag is most significant in high-wind regions to the right of the storm track. These processes are modulations on the maximum-wave region and tend to occur several hours after the peak wind events, depending on the storm translation velocity. The translation speed of the storm is important. The directional variation between local winds and wind-generated waves within rapidly moving storms that outrun the waves is notably different from that of trapped waves, when the dominant waves' group velocity approximates the storm translation speed. While wave drag and spray can increase or reduce the magnitudes of wind and significant wave height, their nondirectional formulations allow them to have little apparent effect on the directional wave spectra.

1. Introduction

Under high-wind conditions, rapidly varying winds continuously generate young waves and enhanced surface stress. Sea spray associated with breaking waves is ejected into the lower level of the atmosphere. Sea spray and spume can enhance the air–sea enthalpy exchange (Andreas and Emanuel 2001; Wang et al. 2001) and make the interaction between the sea and air in the surface boundary layer more complex (Doyle 2002). However, Emanuel (1995) showed that if estimated values of the exchange coefficients at 20 m s^{-1} are applied at higher wind speeds, maintaining a storm of much greater than marginal hurricane intensity would be impossible. Thus, sea spray is a possible mechanism to enhance the air–sea enthalpy exchange at high wind speeds (Andreas and Emanuel 2001) and to maintain a realistic boundary layer structure (Fairall et al. 1994).

We suggest that the heat and moisture transfer mediated by sea spray is also an important process for accurate simulations of ocean waves.

Although recent studies of the impact of wave-induced drag and sea spray processes, as separate factors on air–sea fluxes and storm evolution, have made progress, their collective impact has received less attention. In a companion paper (Zhang et al. 2006), we considered the role of waves and sea spray in midlatitude storms, showing that in high-wind regions (winds exceeding 25 m s^{-1}), spray evaporation can cause the lower part of the atmosphere to experience cooling and moistening. These processes create favorable conditions for storm intensification because the resulting increase in the air–sea temperature difference tends to destabilize the surface layer and enhance the convergence and upward transportation of mass and moisture from the surface.

By comparison, momentum fluxes related to wave drag are important over regions of the storm where young, newly generated waves are prevalent and represent the transfer of atmospheric energy from the winds into the ocean surface. Wave drag is important

Corresponding author address: Dr. William A. Perrie, Bedford Institute of Oceanography, P.O. Box 1006, 1 Challenger Dr., Dartmouth, NS B2Y 4A2, Canada.
E-mail: perriew@dfo-mpo.gc.ca

during the rapid-development phase of the storm, and it decreases in areas where storm waves reach maturity. The collective influence of spray and waves on storm development depends on their occurrence in the early stages of a storm's rapid-intensification phase and their spatial distribution with respect to the storm center.

Previous studies (Doyle 1995; Lionello et al. 1998; Lalbeharry et al. 2000; Desjardins et al. 2000; Zhang and Perrie 2001) have indicated that the impact of atmosphere–wave coupling on the sea state tends to be greater than the impact on the atmosphere. Janssen et al. (2002) suggested that enhanced surface roughness may not always lead to decay in storm intensity because heat fluxes may be enhanced in association with vortex stretching, with concomitant deepening of the low. Lionello et al. (1998), Doyle (2002), and Lalbeharry et al. (2000) suggested that significant wave height has a tendency to be overpredicted in uncoupled atmosphere–ocean wave simulations when winds are overestimated. Thus, a coupled atmosphere–ocean system can enhance the accuracy of forecasting significant wave height, in the sense that wind speed is decreased because of a younger and rougher sea surface. This is an important problem because uncertainty in the winds is an ongoing concern in operational marine forecasts.

Storm-induced waves are complex and rapidly varying in time and space. The effective fetch of wave growth is modulated by the motion of the storm. The curvature of the wind field limits the fetch, but waves that propagate in the direction of the storm's motion remain under the influence of aligned winds for longer effective time and distance. Bowyer and MacAfee (2005) demonstrated that enhanced fetch can produce notably high waves even for rather modest storm intensities, because there is greater time to pump energy into the waves from the wind. Young (2003) suggested that the wave field tends to be more asymmetric than the corresponding wind field, mainly because of the “extended fetch” that exists to the right of a translating hurricane. Thus, storm translation speed (TS) is an important factor in determining the height and spatial distribution of wave fields.

Moon et al. (2003) suggested that rapid-storm translation tends to cause the peak storm waves to lag behind the corresponding peak winds. They also found that hurricane-generated wave fields are mostly determined by the distance from the hurricane center, the radius of maximum wind, and the hurricane translation speed. For a rapidly moving hurricane, the dominant wave direction may be dominated by trapped-wave-type resonance, while for a slowly moving hurricane, the direction of the largest waves is mainly determined by location relative to the storm center.

The primary goal of this study is to evaluate the influence of sea spray and wave drag on storm-induced surface waves in relation to the wind field structure and storm translation speed. The coupled atmosphere–wave–sea spray model used by Zhang et al. (2006) is applied, as described in section 2. Storm cases are described in section 3. The influence of spray, wave drag, and storm translation speed on significant wave height, variations in the wind fields, and the directional wave spectra are examined in section 4. Conclusions are given in section 5.

2. Model description and experimental design

The Mesoscale Compressible Community atmospheric model (MC2; version 4.9.3) is used in all numerical simulations. The MC2 is coupled with the WAVEWATCH III ocean wave model (hereafter WW3; version 1.18) and a standard bulk algorithm for turbulent air–sea fluxes with a high-wind sea spray formulation.

a. Atmospheric model

The MC2 is nonhydrostatic, fully elastic, and state-of-the-art, solving the full Euler equations on a limited-area Cartesian domain (Benoit et al. 1997). Semi-Lagrangian advection and a semi-implicit time-differencing dynamic scheme are used, allowing MC2 to achieve high-quality storm simulations over a wide range of conditions (McTaggart-Cowan et al. 2001; Zhang et al. 2006). The model is implemented on a latitude–longitude projection, on the domain of 25° to 58°N and 40° to 80°W, with 30 vertical layers (11 vertical levels within PBL and the lowest model level at 18 m), a 0.25° horizontal resolution, and 600-s integration time steps. Lateral boundary and initial conditions use Canadian Meteorological Centre (CMC) analysis data. Monin–Obukhov similarity theory is used for the surface fluxes above the sea. The Kain–Fritsch scheme (Kain and Fritsch 1993) is used for deep cumulus convection. Associated boundary layer, turbulent kinetic energy (TKE), and vertical diffusion formulations are described by Benoit et al. (1997).

b. Ocean wave model

The WW3 (Tolman and Chalikov 1996; Tolman et al. 2002; Komen et al. 1994) was implemented on the same domain as the MC2, also with a 0.25° horizontal resolution. The model simulates directional wave spectra in terms of wavenumber–direction bands by solving the well-known spectral action balance equation, and it explicitly parameterizes the energy input to waves by wind S_{in} , wave dissipation S_{ds} , and wave–wave interactions S_{nl} .

c. Air–sea fluxes

Heat, moisture, and momentum can be transferred across the air–sea interface through the interfacial or turbulent fluxes, expressed as bulk turbulent flux parameterizations. The MC2 uses Monin–Obukhov similarity theory for the interfacial fluxes of momentum τ , sensible heat H_S , and latent heat H_L :

$$\tau = \rho_a C_d U_{zl}^2, \quad (1)$$

$$H_S = \rho_a c_{pa} C_H U_{zl} (\theta_o - \theta_{zl}), \quad \text{and} \quad (2)$$

$$H_L = \rho_a L_v C_E U_{zl} (q_o - q_{zl}). \quad (3)$$

Here U , θ , and q are the mean wind speed, potential temperature, and specific humidity, respectively; ρ_a is the air density; c_{pa} is the specific heat of air at constant pressure; and L_v is the latent heat of vaporization of water. Subscripts zl and o are the lowest atmospheric model level and the ocean surface, respectively. Positive heat fluxes are upward.

There is a high level of uncertainty in high-wind conditions because field data are difficult to obtain. In uncoupled simulations over the sea, the atmospheric model parameterizes the momentum roughness length Z_{0m} by the Charnock (1955) relation

$$Z_{0m} = \beta u_*^2 / g, \quad (4)$$

where β is the Charnock parameter taken as 0.018. This represents mature sea conditions. In coupled simulations (described in the following sections), Z_{0m} is assumed to be sea-state dependent. This assumption follows the suggestion by Smith et al. (1992) that younger waves satisfy the following relation:

$$Z_{0m} = 0.48 \left(\frac{C_P}{u_*} \right)^{-1} \frac{u_*^2}{g}, \quad (5)$$

where β in Eq. (4) is generalized to include wave age C_P/u_* in Eq. (5), C_P is the phase velocity at the wave spectrum peak, g is gravitational acceleration, and u_* is friction velocity. As waves mature, C_P/u_* increases and Z_{0m} decreases.

Desjardins et al. (2000), Zhang and Perrie (2001), and Janssen et al. (2002) show that Eq. (5) gives similar results to those of the wave-induced stress formulation of Janssen (1991). In the limit when $C_P/u_* \geq 26$, the Charnock Z_{0m} relation is used in Eq. (5). Motivated by Emanuel (2003), the high wind speed laboratory data of Donelan et al. (2004), and the field data of Powell et al. (2003), we set the high-wind limit for Z_{0m} to 0.0034 m when 10-m reference winds (U_{10}) exceed 30 m s⁻¹. Our upper limit for Z_{0m} corresponds to the limiting drag coefficient of 0.0025 suggested by Donelan et al. (2004)

for high winds in excess of 30 m s⁻¹, which is approximately consistent with Powell et al. (2003).

Figure 1a shows that for conditions experienced during the storm cases considered in this paper, the Z_{0m} formulation in Eq. (5) with the high-wind constraint corresponds to a drag coefficient variation with U_{10} that is consistent with hurricane observations (Powell et al. 2003), theoretical estimates (Moon et al. 2004), and observations (Smith et al. 1992; Drennan et al. 2003). When the high-wind condition is modified slightly to $Z_{0m} = 0.005$ m when $U_{10} > 30$ m s⁻¹, peak drag coefficient values increase very slightly (not shown). Simulations were also completed in Fig. 1a using the formulations of Drennan et al. (2003) and Drennan (2006), but they did not produce any notable modifications [compared to the Humidity Exchange over the Sea's (HEXOS) experiment; described by Smith et al. (1992) formulation of Eq. (5)] of the storm simulations.

Figure 1b shows the variation of Charnock parameter β as a function of inverse-wave age from model runs subdivided according to the development phase of the storms. This confirms the overall agreement of the model system to roughness parameterizations given in Eqs. (4) and (5).

The limit $Z_{0m} = 0.0034$ approximates the drag coefficient results of Donelan et al. (2004) and Powell et al. (2003) when $U_{10} > 30$ m s⁻¹, as shown in Fig. 1a. The data of Donelan et al. (2004) are from laboratory experiments, and the hurricane data of Powell et al. (2003) were collected by dropsondes in continuously changing high-wind conditions. When $U_{10} < 30$ m s⁻¹, both datasets are biased low compared to measurements by Drennan et al. (2003), Smith et al. (1992), and Large and Pond (1981). Some of the difference may result from the continuously changing swell interactions with local wind-generated waves (e.g., in the data of Powell et al. 2003). Drennan (2006) suggests that for the open-ocean fetch-limited wave growth and counter-swell, the drag coefficient is larger than in corresponding following-swell cases. The results of Smith et al. (1992) were obtained for fetch-limited growing waves in the absence of swell. Moreover, estimates from our simulations in Fig. 1b were obtained from open ocean locations far from the coastline, with wind directions collinear with wave directions in cases where swell is absent, following the data analysis used by Smith et al. (1992).

Finally, since there is no consensus that enthalpy transfer has sea-state-dependent roughness lengths for thermal fluxes, Z_{0t} , the roughness length for temperature, and Z_{0q} , the roughness length for humidity, are simply fixed (4×10^{-5} m) in MC2 runs (Doyle 2002).

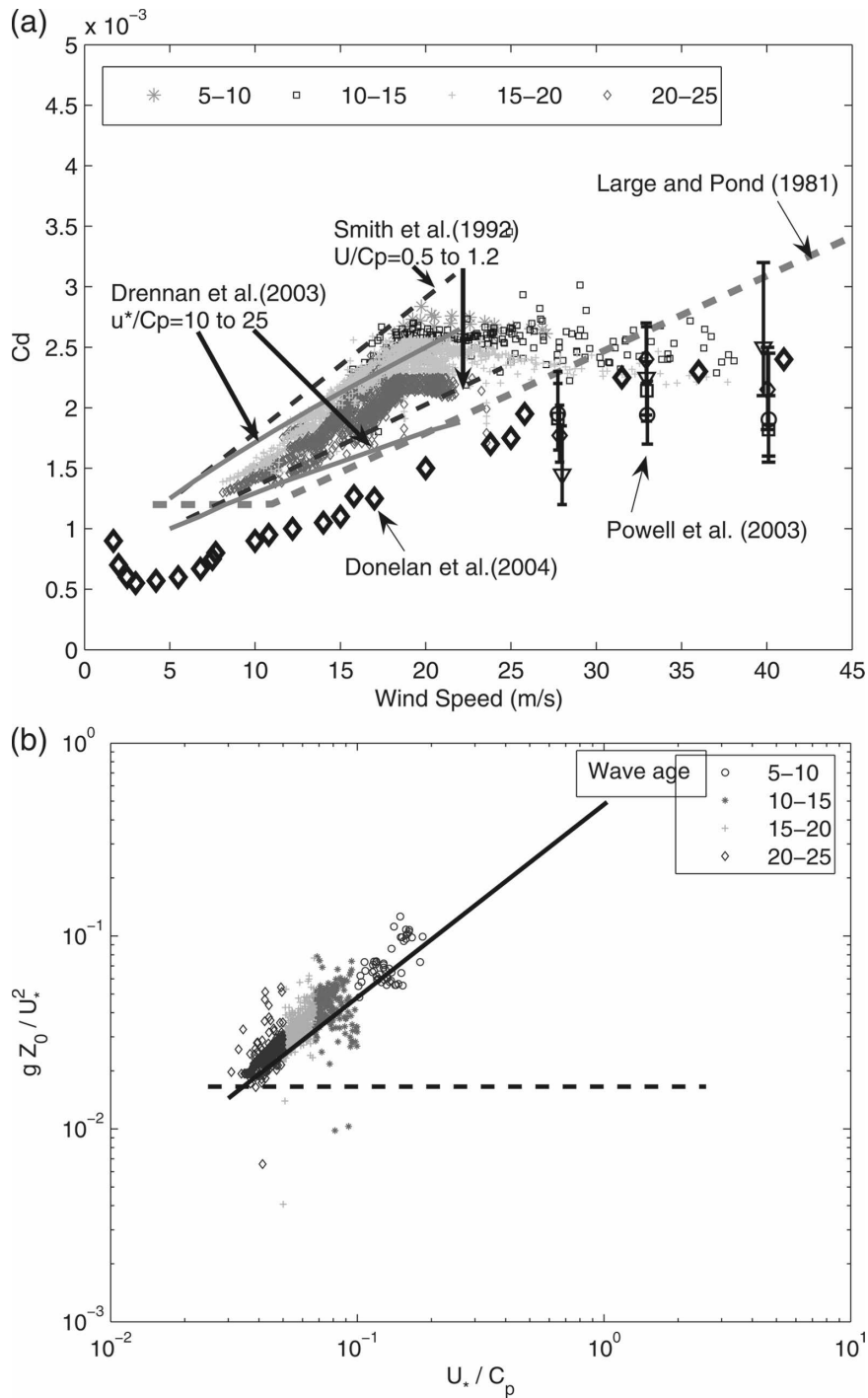


FIG. 1. (a) Comparison of observed neutral drag coefficient C_d from Powell et al. (2003) (circles, diamonds, squares, and triangles; vertical bars showing 95% confidence); Large and Pond (1981) (heavy dashed line); Donelan et al. (2004) (bold diamonds); and C_d from coupled model results from MC2, grouped according to different wave ages [Eq. (5)], with the restriction that when $U_{10} > 30 \text{ m s}^{-1}$ we limit $Z_0 = 0.0034 \text{ m}$. Dark dashed line and light solid lines indicate C_d associated with young and fully developed sea states, following Smith et al. (1992) and Drennan et al. (2003), respectively. (b) Charnock parameter β versus inverse-wave age compared with Eqs. (4) (solid line) and (5) (dashed line).

d. Sea spray

Over the sea, MC2's interfacial momentum and heat fluxes are calculated using the Monin–Obukhov theory leading to a bulk formulation based on turbulent transfer coefficients. These depend on empirical similarity functions ψ_m and ψ_h as well as on roughness lengths for wind speed, temperature, and humidity— Z_{0m} , Z_{0t} , and Z_{0q} , respectively. However, Andreas's (2003) bulk spray flux algorithm is derived by subtracting estimates of the interfacial heat fluxes from HEXOS measurements of the total heat fluxes. He used the interfacial heat flux parameterization of Liu et al. (1979), which is the basis for the Tropical Ocean and Global Atmosphere Coupled Ocean–Atmosphere Response Experiment (TOGA COARE; version 2.6) algorithm (Fairall et al. 1996). Thus the spray flux is the residual and is specifically tuned to this TOGA COARE-type parameterization.

Total momentum τ_T as well as latent $H_{L,T}$ and sensible $H_{S,T}$ heat fluxes, which constitute the boundary conditions at the lowest model level, are obtained by adding the corresponding bulk interfacial (τ , H_L , H_S) and spray fluxes (τ_{SP} , $Q_{L,SP}$, $Q_{S,SP}$), following Andreas and DeCosmo (1999), Andreas and Emanuel (2001), and Andreas (2003):

$$\tau_T = \tau + \tau_{SP}, \quad (6)$$

$$H_{L,T} = H_L + Q_{L,SP}, \quad \text{and} \quad (7)$$

$$H_{S,T} = H_S + Q_{S,SP}. \quad (8)$$

Andreas's (1992) spray flux model suggests that droplets whose initial radii are 100 and 50 μm are leading indicators of the spray sensible heat and the spray latent heat (Andreas 1992, 1995, 1998). Andreas (2003) therefore assumed that these droplets are the bellwethers of their respective spray fluxes and modeled the heat fluxes as

$$Q_{S,SP} = \rho_w c_w (\theta_0 - T_{\text{eq},100}) V_S(u_*) \quad \text{and} \quad (9)$$

$$Q_{L,SP} = \rho_w L_v \left[1 - \left(\frac{r_{\text{eq},50}}{50 \mu\text{m}} \right)^3 \right] V_L(u_*), \quad (10)$$

where ρ_w is seawater density and c_w is the seawater-specific heat; $T_{\text{eq},100}$ is the equilibrium temperature of spray droplets with a 100- μm initial radius (Andreas 1995); and $r_{\text{eq},50}$ is the equilibrium radius of droplets with a 50- μm initial radius. Wind functions V_S and V_L depend on u_* and tune Eqs. (9) and (10) to HEXOS data (Andreas and DeCosmo 2002; Andreas 2003), yielding

$$V_S(u_*) = 1.65 \times 10^{-6} u_*^3 \quad \text{and} \quad (11)$$

$$V_L(u_*) = 4.75 \times 10^{-8} u_*^3. \quad (12)$$

Units for $Q_{L,SP}$, $Q_{S,SP}$, H_S , and H_L are in watts per squared meter when u_* is in units of meters per second. Spray-mediated fluxes $Q_{S,SP}$ and $Q_{L,SP}$ increase much more rapidly with U_{10} than do the interfacial fluxes: for example, when U_{10} exceeds 30 m s^{-1} , $Q_{L,SP}$ and $Q_{S,SP}$ exceed H_L and H_S , respectively (Perrie et al. 2005).

When spray droplets are ejected into the air, they quickly accelerate to the local wind speed, extracting momentum from the wind and slowing it. Falling back to the sea, they transfer momentum and influence the wind speed profile, the atmospheric momentum profile, and the surface stress, which can be estimated according to Andreas (1998, 2003) and Andreas and Emanuel (2001) as

$$\tau_{SP} = 6.2 \times 10^{-5} \rho_w u_*^4. \quad (13)$$

Because Eq. (13) varies as the fourth power of u_* , it becomes larger than the interfacial stress ($\rho_a u_*^2$) when u_* is about 4 m s^{-1} or when U_{10} is larger than about 65 m s^{-1} . As wind speeds are rarely above 40 m s^{-1} in our simulations, the spray stress is negligible.

e. Coupling formulation and experimental design

Because the model time steps for MC2 and WW3 are 600 and 900 s, respectively, the coupling time step is 1800 s. Between coupling time steps, the Charnock parameter β in MC2 remains the same. At every coupling time step, information is exchanged between the atmosphere and the waves: wind speed and direction computed by MC2 are transferred to the WW3, and in turn, C_p computed by WW3 is passed to MC2, allowing for the computation of new Z_{0m} values. Spray-mediated heat fluxes are passed back to MC2 at each MC2 time step.

Four experiments were performed to study wave drag and sea spray impacts on storm-induced waves. The control simulation uses MC2 atmospheric model winds to drive the WW3 waves, assuming the conventional Charnock roughness [Eq. (4)] with no feedback to MC2 and no spray (one-way coupling). The fully coupled (two-way coupled) MC2-wave-spray simulation includes spray-enhanced heat and momentum fluxes and wave-modified stress feedbacks to MC2. Two partially coupled simulations study wave drag and spray competition: 1) coupled MC2-wave run with wave-modified β [Eq. (5)] passed to MC2, but no spray-modified fluxes, and 2) coupled MC2-spray run with no wave-modified β passed to MC2.

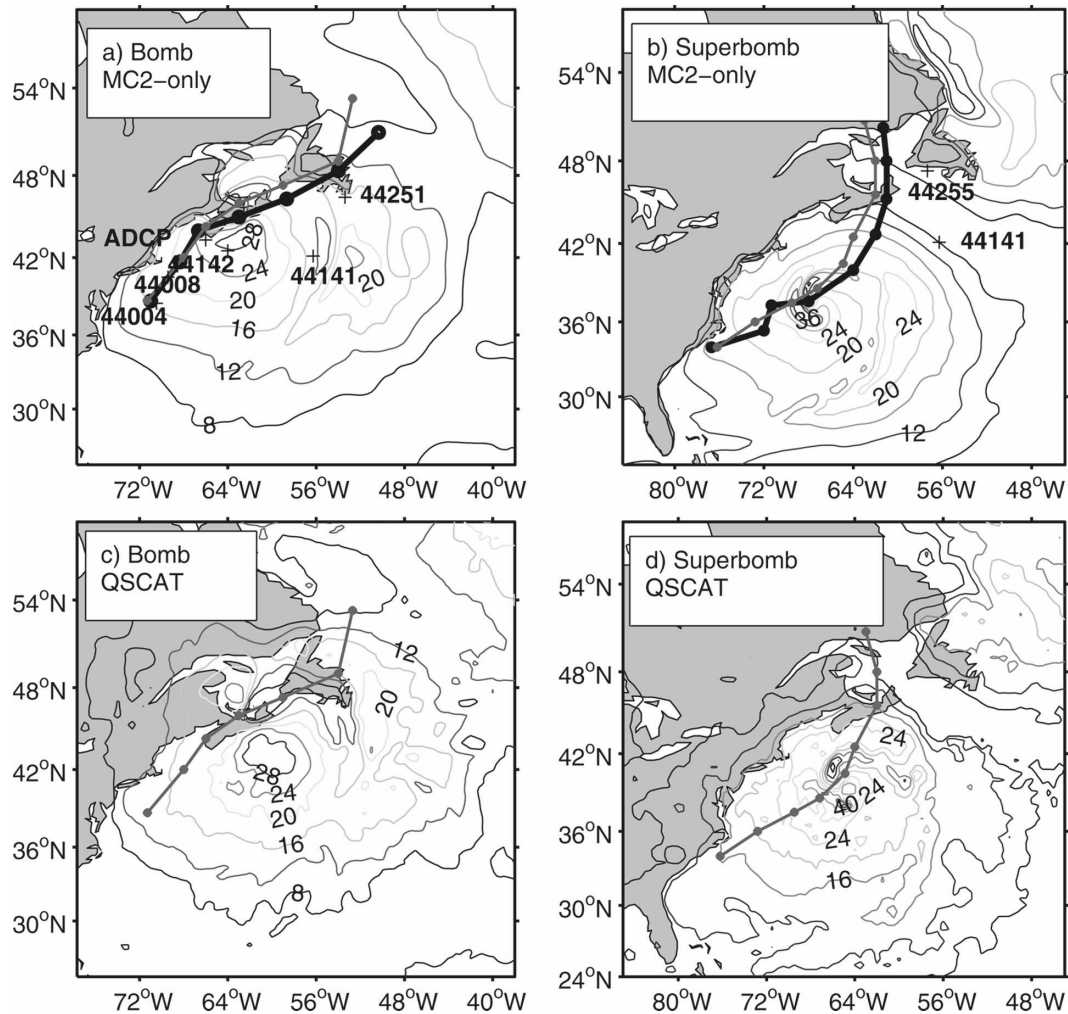


FIG. 2. Comparison of (a) control simulation and (c) QuikSCAT–NCEP-blended wind speed fields (contour, m s^{-1}) during maximum intensity for the bomb (0600 UTC 14 Jan 2002) and (b), (d) the superbomb (0600 UTC 21 Jan 2000). Six-hourly storm track starts from 1200 UTC 13 Jan 2002 for the bomb and 1200 UTC 20 Jan 2000 for the superbomb; CMC-analysis track is indicated by filled circles; and simulated storm track is indicated by open circles. ADCP instrument location and buoys 44004, 44008, 44141, 44142, and 44251 are included in (a), and buoys 44141 and 44255 in (b).

3. Storm cases

As a storm case, the 2002 January “bomb” followed the typical development pattern of North Atlantic winter storms. It was a meteorological bomb that started as a rapidly intensifying low pressure system off the coast of North Carolina at 1200 UTC 13 January 2002 (storm track in Fig. 2a). It deepened over the next 12 h and moved northeastward, generating high winds and 18-m seas at National Data Buoy Center (NDBC) buoys in the Gulf of Maine and off eastern Canada. Nearing Nova Scotia at 0000 UTC 14 January 2002, maximum sustained winds were 30 m s^{-1} and central sea level pressure (SLP) fell to 962 hPa (Zhang et al.

2006). It continued northeastward, crossed eastern Nova Scotia and Newfoundland, and dissipated by 15 January 2002.

The “superbomb” was similar to the bomb in that it developed off Cape Hatteras, North Carolina, and deepened explosively from 995 hPa at 1200 UTC 20 January to 951 hPa by 1200 UTC 21 January 2000 (storm track in Fig. 2b). At midlevels, CMC analysis suggests that a short wave traveled quickly around the base of a deepening larger-scale trough over the Hudson Bay. The system was under the influence of a jet to its south and west, benefiting from the divergent upper-level forcing associated with the left-exit region. Phase locking occurred, and the vertically stacked system

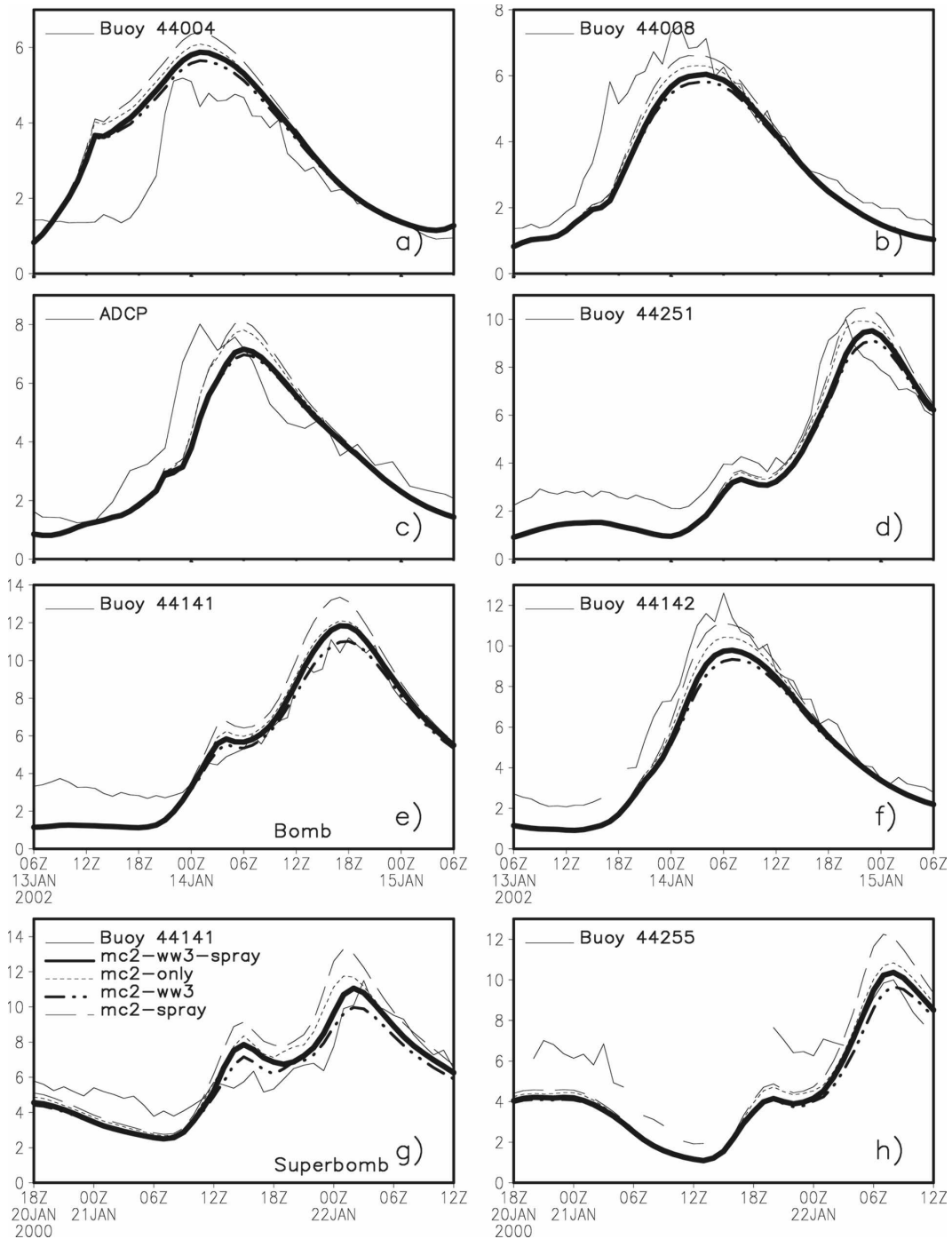


FIG. 3. Time series of observed and simulated significant wave heights (m) at buoy locations and the ADCP location (shown in Fig. 2) for (a)–(f) the bomb and (g), (h) the superbomb.

curled northward under the influence of midlevel flow. Propagating northeastward, the superbomb's peak U_{10} winds reached 45 m s^{-1} near Nova Scotia. It made land-fall at 0000 UTC 22 January 2000 and continued weakening.

4. Results

a. Model verification

Accurate simulation of storm-induced waves depends on realistic winds, accurate specification of the

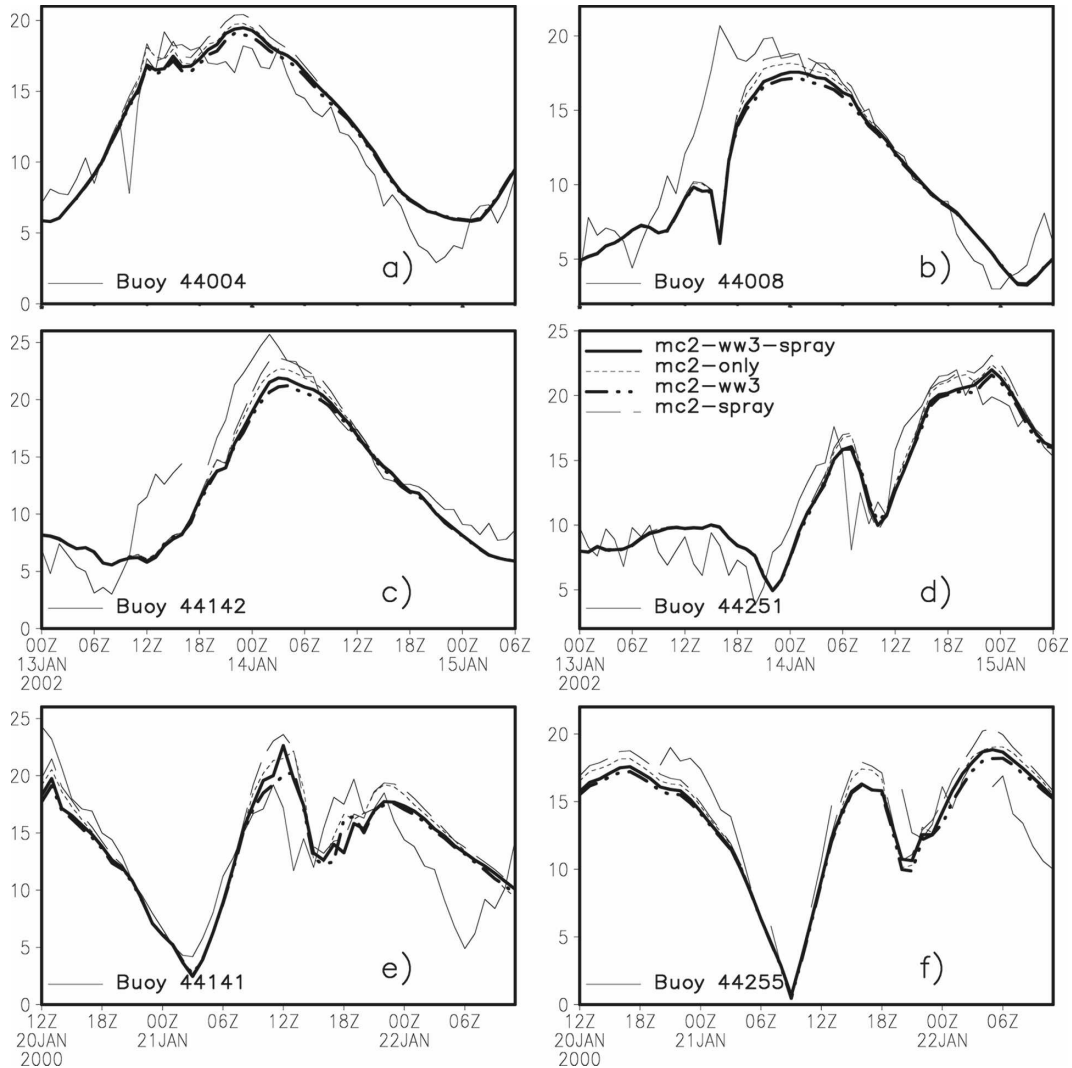


FIG. 4. Comparisons of the wind speeds at 10 m (in m s^{-1}) between observations and simulations at buoys (a)–(d) for the bomb, and (e)–(f) for the superbomb. Legend follows Fig. 3.

radius of maximum wind, and storm translation speed. Shortcomings in synoptic forcing constitute an important cause for the differences between observations and simulations. Figures 2a–d compare control winds from MC2 to those from Quik Scatterometer (QuikSCAT)–National Centers for Environmental Prediction (NCEP) analyses (<http://dss.ucar.edu/datasets/ds744.4/>) at the bomb's peak intensity, at 0600 UTC 14 January 2002 (Figs. 2a,c) and at the superbomb's peak intensity, at 0600 UTC 21 January 2000 (Figs. 2b,d). These plots show that the overall structures from the MC2 control simulation and the QuikSCAT–NCEP analyses are similar, except that simulated storm tracks are slightly biased to the right of the CMC-analyzed tracks. Maximum QuikSCAT–NCEP winds are 30 and 40 m s^{-1} , compared to control winds of 28 and 36 m s^{-1} for the

bomb and the superbomb, respectively. The asymmetric character of the wind structure is evident in both simulated and QuikSCAT–NCEP winds. For the bomb, the simulated radius of maximum U_{10} is smaller than that of QuikSCAT–NCEP. Although the MC2 simulation of the superbomb translates at a slightly faster speed than that in QuikSCAT–NCEP, the high-wind region is very compact, which is consistent with the QuikSCAT–NCEP results.

Overall, MC2 can give good baseline simulations of storm tracks and distributions. As further validation, time series comparisons of simulations and observations for significant wave heights (SVHs), U_{10} , and wind directions at buoy locations (Fig. 2) from the bomb and the superbomb are shown in Figs. 3–5. For example, in Figs. 3g,h, the MC2 control simulation of the super-

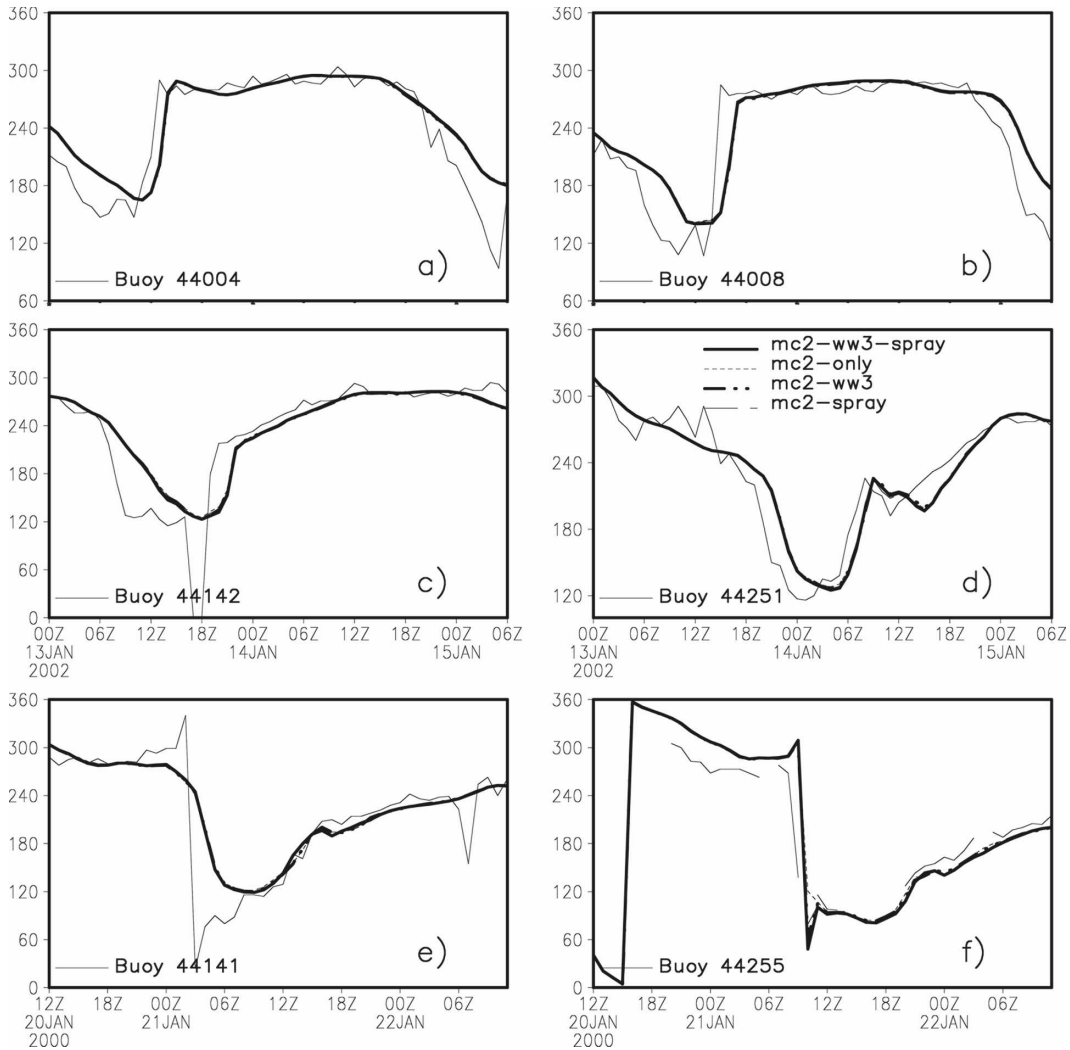


FIG. 5. The same as in Fig. 4, but for wind directions (degrees). The legend is the same as in Fig. 3.

bomb captures the significant wave height variation at the second peak event quite well, in comparison with the observations at buoys 44141 and 44255.

For the bomb, the MC2 control simulation underpredicts the significant wave height time series during the lead-up to the storm peaks at buoys 44008 and 44142 (Figs. 3b,f), whereas significant wave heights at buoy 44141 (Fig. 3e) are overpredicted. The peak significant wave heights at the acoustic Doppler current profiler (ADCP) location (Fig. 3c) and at buoys 44251 (Fig. 3d) and 44004 (Fig. 3a) tend to lag the observations by about 6 h. It is noteworthy that buoys 44008 and 44142 are very close to the areas of rapidly changing wind directions with strong wind field curvature near the storm center, whereas buoy 44141 is located in the open ocean while ADCP and buoy 44251 are near shore. It is important to investigate the variations in significant

wave height underestimations, overestimations, and phase lag in relation to locations within the storm.

The estimated correlation (COR), root-mean-square error (RMSE), and biases in significant wave heights (excluding the model warm-up period) between MC2 control simulations and buoy observations are listed in Table 1. Overall, the correlation is significant at the 95% confidence level, and total significant wave height bias is less than 1.0 m.

Although the total significant wave height biases are lower for the superbomb than for the bomb, RMSE values are slightly higher, because even though our simulation captures the second significant wave height peak, the first significant wave height peak is overpredicted at buoy 44141 and underpredicted at buoy 44255 (Figs. 3g,h). Wave results are always dependent on wind errors. Simulated U_{10} values for the bomb from

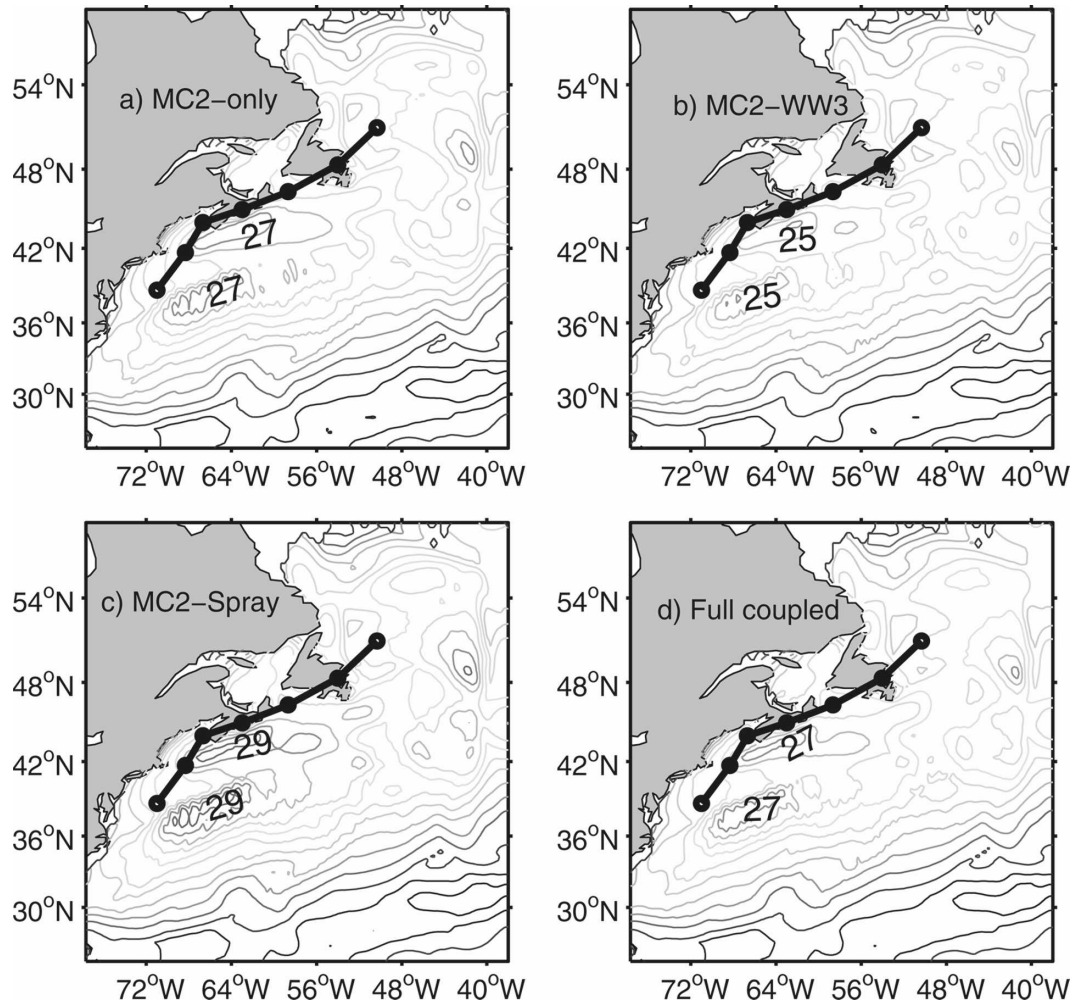


FIG. 6. Swath maps of wind speed (m s^{-1}) for the passage of the bomb with a 2 m s^{-1} interval. Superimposed is 6-hourly storm track starting from 1200 UTC 13 Jan 2002. The swath map represents the maximum wind in every grid point during the passage of the storm.

the uncoupled MC2-only simulation are underpredicted at buoys 44008 and 44142 (Figs. 4b,c), and total biases are about 2 m s^{-1} . At buoys 44004 and 44251 (Figs. 4a–d), simulated U_{10} estimates are quite close to the observations and biases are less than 1 m s^{-1} . Un-

fortunately, there were no U_{10} observations at buoy 44141 or at ADCP during our simulation period.

For the superbomb, total biases are less than 0.5 m s^{-1} at buoys 44141 and 44255 (Figs. 4e,f). Since the simulated wind speed at buoy 44141 overpredicted the

TABLE 1. COR, RMSE, bias for significant wave height (H_S), and wind speed at 10 m (U_{10}) between observations and MC2-control simulation. Here, N is the number of degrees of freedom. Units for RMSE and bias are meters.

	January bomb						Superbomb							
	44004		44008		ADCP	44141	44142		44251		44141		44255	
	U_{10}	H_S	U_{10}	H_S	H_S	H_S	U_{10}	H_S	U_{10}	H_S	U_{10}	H_S	U_{10}	H_S
COR	0.81	0.83	0.77	0.92	0.86	0.98	0.83	0.94	0.78	0.97	0.72	0.82	0.64	0.85
RMSE	1.84	1.33	4.09	0.99	1.15	1.09	3.98	1.15	2.13	1.08	4.64	2.04	3.72	1.46
Bias	0.93	0.95	-2.05	-0.67	-0.32	0.03	-2.24	-0.90	0.33	-0.46	0.43	-0.35	-0.18	-0.65
N	58	43	58	43	43	43	58	43	58	43	49	37	49	37

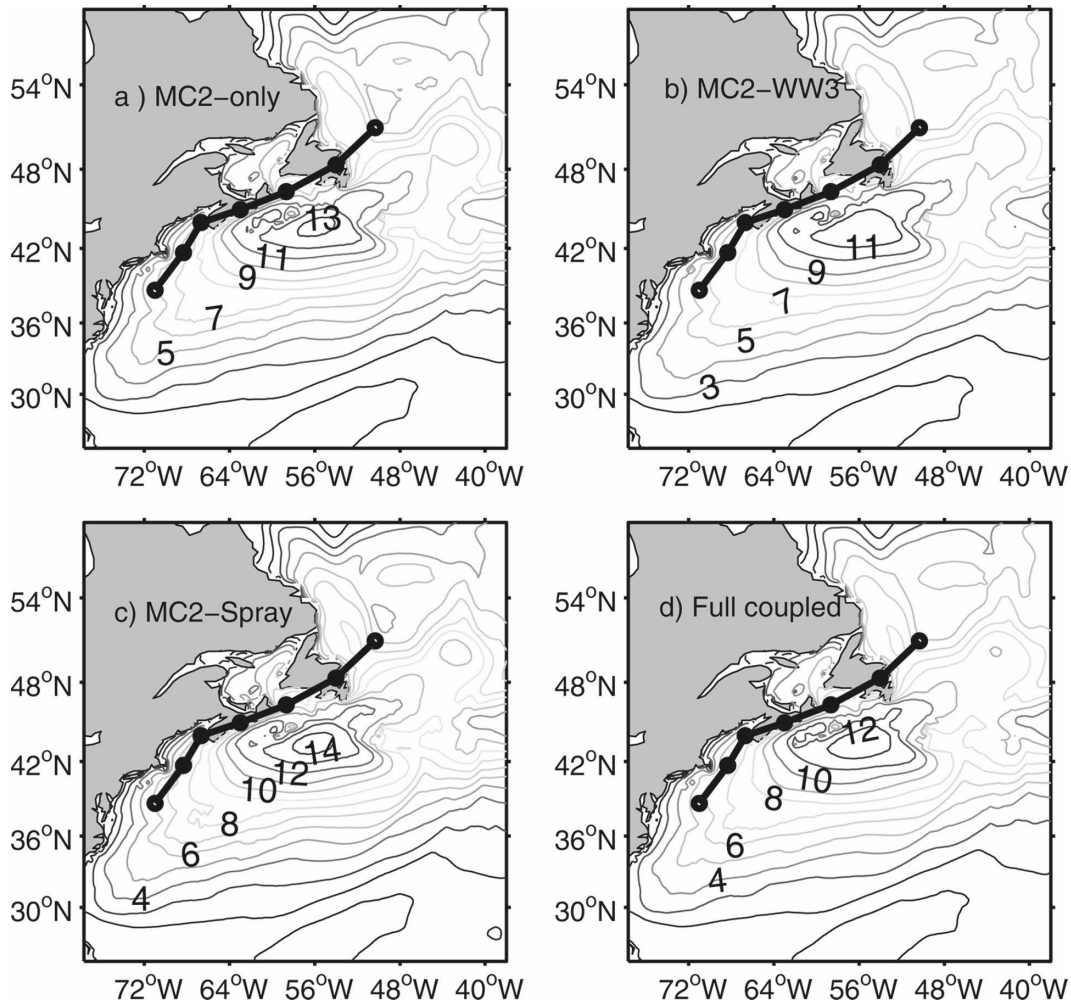


FIG. 7. As in Fig. 6, swath maps of significant wave heights (m) from the passage of the bomb at 1-m intervals.

first peak in the wind time series, the RMSE is therefore slightly higher. This is consistent with the simulated significant wave height time series. Estimates of the time series of wind direction from the four simulations do not differ appreciably and basically agree with observations (Fig. 5). Very little simulated sensitivity with respect to spray or waves is exhibited.

b. Baseline simulation of wind and wave fields

Walsh et al. (2002) suggest that the wave field in the vicinity of a hurricane may be well behaved in the sense that it can sometimes be modeled by a few parameters, such as the maximum wind speed, the radii of the maximum gale-force winds, and the recent movement of the storm. Figures 6 and 7 show the swath isolines of simulated winds and the significant wave height for the bomb, respectively. Similar results are shown in Figs. 8 and 9 for the superbomb. Swath maps represent the

maximum value at every grid point during the passage of the storm; all wind maxima appear in the right forward quadrant along the storm track.

In the bomb, although high winds are sustained from 1800 UTC 13 January to 0600 UTC 14 January 2002 (discussed later in Fig. 10a), the maximum significant wave heights following the passage of the storm are between 7.5 and 11 m during this period (not shown). Thus, from Figs. 6a and 7a we infer that peak waves of 13 m occur a few hours after peak winds of 27 m s^{-1} (0000–0600 UTC 14 January 2002) in the bomb. For the superbomb, maximum winds (36 m s^{-1}) occur at 0600 UTC 21 January 2000, while 17-m waves also appear a few hours later (Figs. 8a, 9a).

The lag in the peak waves behind the peak storm winds occurs because the storm translation speed exceeds the group velocity of the dominant waves (Bowler and MacAfee 2005; Moon et al. 2003; Young 2003).

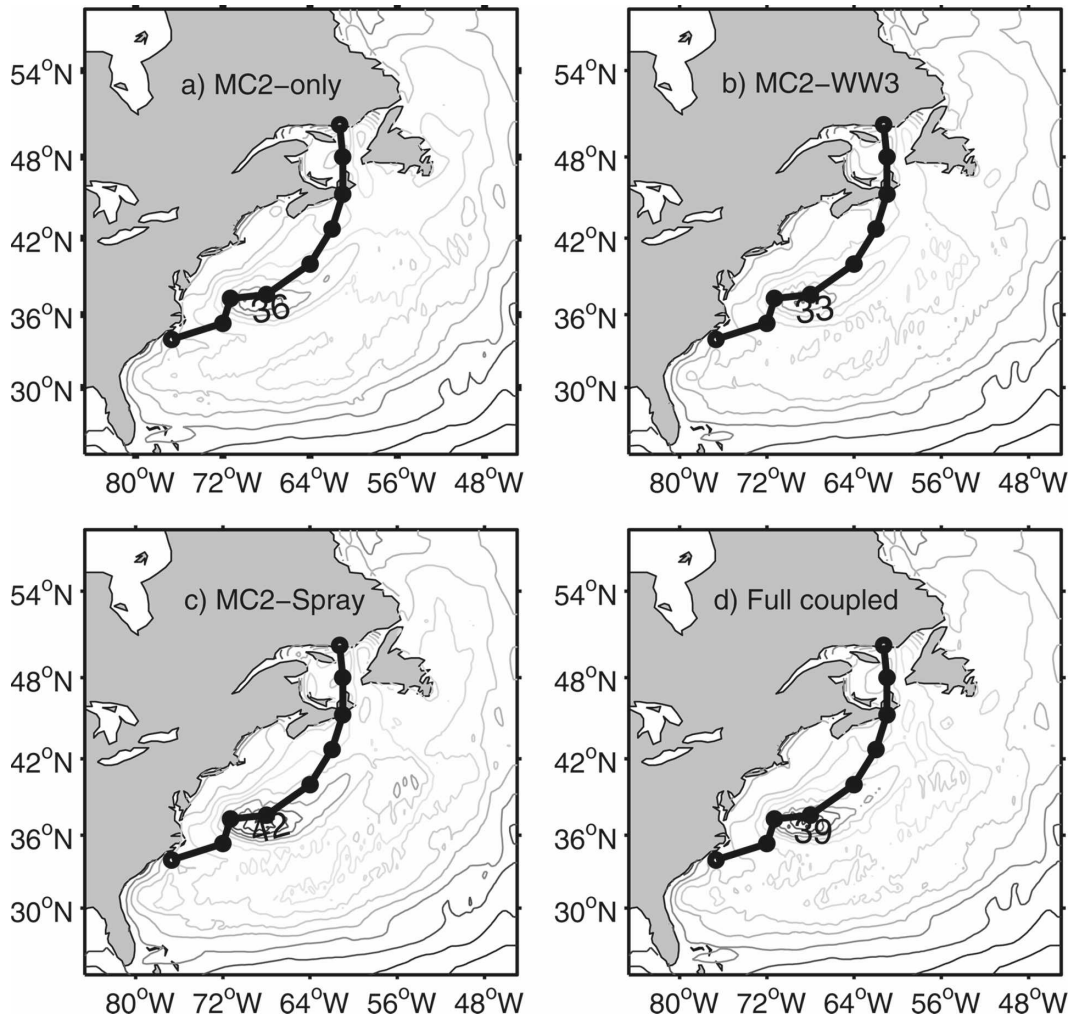


FIG. 8. Swath maps of wind speed (m s^{-1}) from the passage of the superbomb at 3 m s^{-1} intervals. In each panel the 6-hourly storm track is superposed, starting at 1200 UTC 20 Jan 2000.

This has definite effects on significant wave heights generated by the storm. For example, at 0000 UTC 14 January 2002, the bomb's translation speed slows and tends to approach the group velocity of the dominant waves (Figs. 6a, 10a), allowing extra time for wind to pump energy into the waves, and this leads to enhanced significant wave heights over the southern Grand Banks several hours later. As another example, at two instances, 0000 UTC 21 January and 0000 UTC 22 January 2000, the superbomb's translation speeds are comparable to the group velocity of the dominant waves (Fig. 10b). However, during the latter instance, the storm's translation speed is decelerating and significant wave height levels build dramatically to $\sim 4 \text{ m}$ higher than significant wave heights during the former accelerating stage at 0000 UTC 21 January 2000, which has the strongest winds (Fig. 9a).

c. Effects of spray and waves on wind and wave height

The mechanisms of sea spray and wave drag roughness have differing influences on storm development (Zhang et al. 2006). These processes affect the winds that drive the waves and, in turn, the wave feedbacks on the winds and the storm. Wave drag effects are related to friction-induced sea surface roughening and dissipation of momentum; spray influences tend to increase intensity of the storm system because of spray evaporation (Fig. 4). Thus, compared to buoy measurements of significant wave heights (Fig. 3), simulations with explicit wave drag effects (MC2 wave) tend to have reduced significant wave heights compared to those from the control (MC2 only) simulation, whereas sea spray (coupled MC2-spray runs) tends to increase sig-

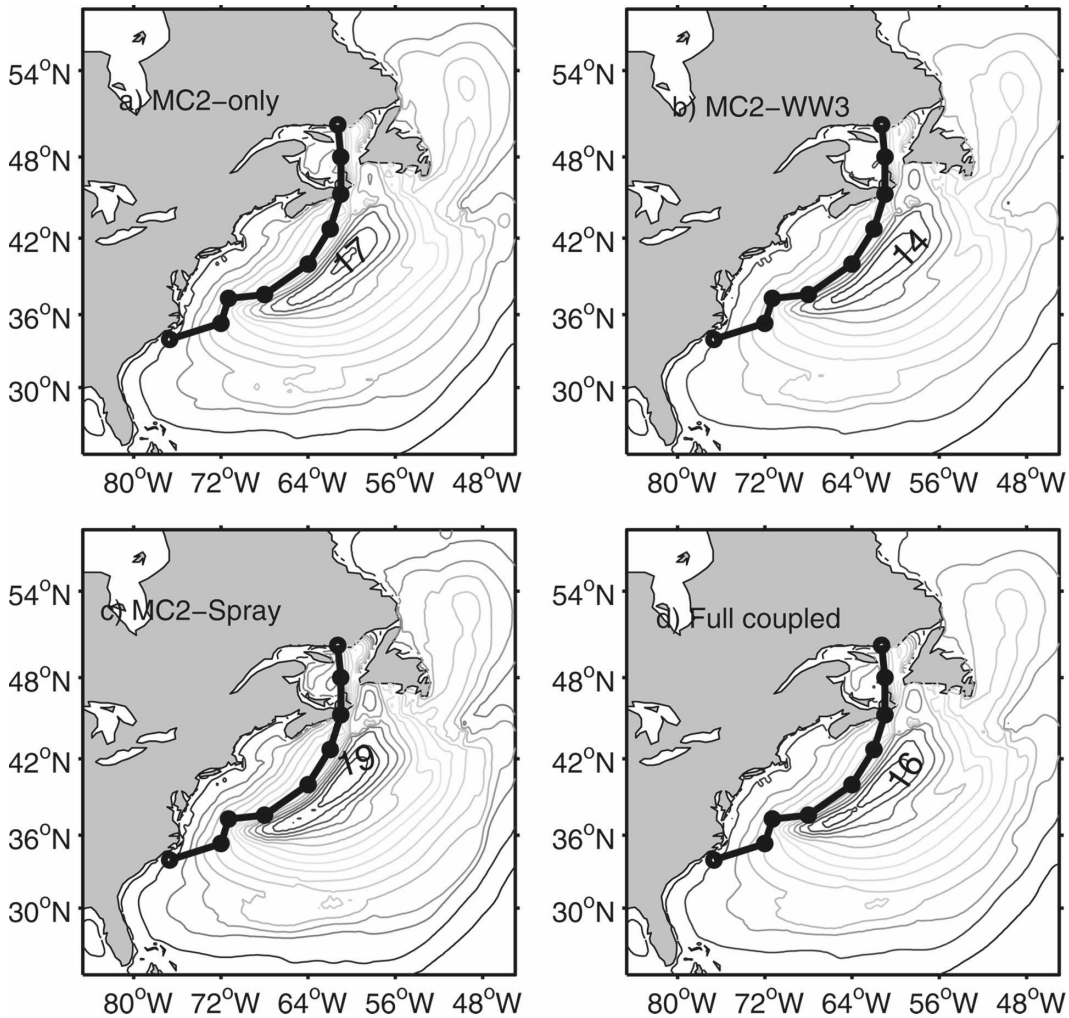


FIG. 9. Swath maps of significant wave heights (m) with the passage of the superbomb at 1-m intervals.

nificant wave heights. Swath plots of wind speed and significant wave height from the MC2-wave and MC2-spray simulations show the same features (Figs. 6b,c; 7b,c; 8b,c; and 9b,c).

The maximum reductions in wind speed due to wave drag are -2 and -3 m s^{-1} for the bomb and the superbomb, respectively. Maximum increases in wind speed due to spray are $+2$ and $+6 \text{ m s}^{-1}$ for the bomb and the superbomb, respectively. For significant wave height, the maximum wave drag effects are -2 and -3 m for the two storms, respectively. Maximum spray effects are $+1$ and $+2 \text{ m}$ for the two storms, respectively. The effects on waves lag the corresponding effects on winds by about 6–12 h because of the dependence of wave development on storm translation speed, as mentioned in section 4b, and the wind forcing history (Moon et al. 2004). The corresponding spatial distributions of wind and significant wave heights from the control simula-

tion and the difference fields, between MC2-wave, MC2-spray, fully coupled, and control simulations, are shown in Figs. 11 and 12. These plots correspond to the instance in each storm of maximum influences of wave drag and spray on significant wave height. In both storms, the highest waves coincide with the maximum winds and appear in the rear right quadrant relative to the storm center (Figs. 11a, 12a). At these instances, the storm centers are relatively distant from the regions where the maximum winds and waves occur, compared with the distances occurring at the peaks of the storms: for example, 0000 UTC 14 January 2002 for the bomb and 0600 UTC 21 January 2000 for the superbomb (not shown).

Moreover, high waves occur near the storm centers as well as in extended spiral bands in the storms' right forward quadrants dominated by the curvature of the wind fields. As a result of the rapid variation in winds in

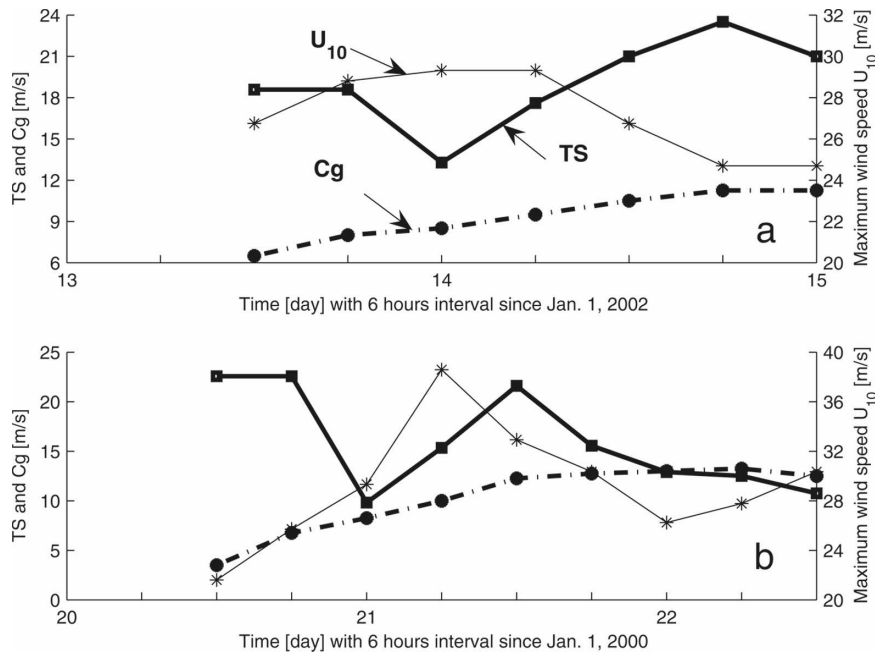


FIG. 10. TS, mean group velocity (C_g) of the dominant wave, and maximum wind speed from the uncoupled MC2-only run for (a) the bomb in January 2002 and (b) the superbomb in January 2000. These values were deduced from locations that move with the storm centers, as the storms propagate along their storm tracks.

these regions, the sea is rough, young waves are continuously being generated, wave drag is high, and sea spray is being ejected into the lower atmosphere. The influence of wave drag or spray on wind speed in these spiral regions is at least as significant as in the maximum wind regions close to the storm centers (shaded areas in Figs. 11b,c; 12b,c). The MC2-wave simulations suggest that the youngest ocean waves have maximum values for the Charnock parameter [defined by Eq. (5)], which for the bomb and the superbomb (Fig. 13) are in excess of 0.04 and 0.035, respectively. These values occur in the extended right and forward quadrants, which is consistent with the growth of high waves in the spiral bands shown in Figs. 11 and 12. The Charnock parameter from the MC2-spray simulation has the same patterns as those of the MC2-wave simulation, with ~ 0.005 higher maximum values (not shown). However, it is notable that the effect of wave drag and spray on significant wave height (Figs. 11b,c; 12b,c) is greater in the high-wind region, regardless of the complexity of the sea state in regions of strong wind curvature. Maximum reductions are 1.6 m or $\sim 12.3\%$ for the bomb and 2.8 m or $\sim 15.3\%$ for the superbomb. Corresponding maximum increases are 1.2 m or $\sim 9.2\%$ for the bomb and 2.4 m or $\sim 14.6\%$ for the superbomb.

Because the influences of spray and wave drag are competitive, significant wave height estimates from

fully coupled simulations may be close to those of the control (MC2 only) runs (Figs. 3e–h), depending on the spray's tendency to intensify the storm and the wave drag's deintensifying tendency (Zhang et al. 2006). Clearly, if winds from the uncoupled MC2 run are biased low, the coupled MC2-wave simulation can be even more biased, as shown at buoys 44008, 44251, and 44142 (Figs. 3b,d,f). If the uncoupled MC2 run is biased high, inclusion of spray tends to cause further high bias in significant wave heights, as shown at buoys 44004 and 44141 (Figs. 3a,e). Finally, at the superbomb's second peak, the largest significant wave height increase due to spray is comparable to the reduction due to wave drag, giving results from the fully coupled run that are close to observations (Figs. 3g,h).

d. Effects on dominant-wave direction

The curvature in the hurricane wind fields causes misalignment of the strongest local winds and the dominant propagating waves. In their analysis of Hurricane Bonnie, Moon et al. (2003) found that when the storm was moving slowly in the open ocean, dominant waves are typically found to the right of the wind direction, except near the hurricane center. We compare the directions between maximum winds and dominant waves from the MC2-wave simulations in the bomb and the

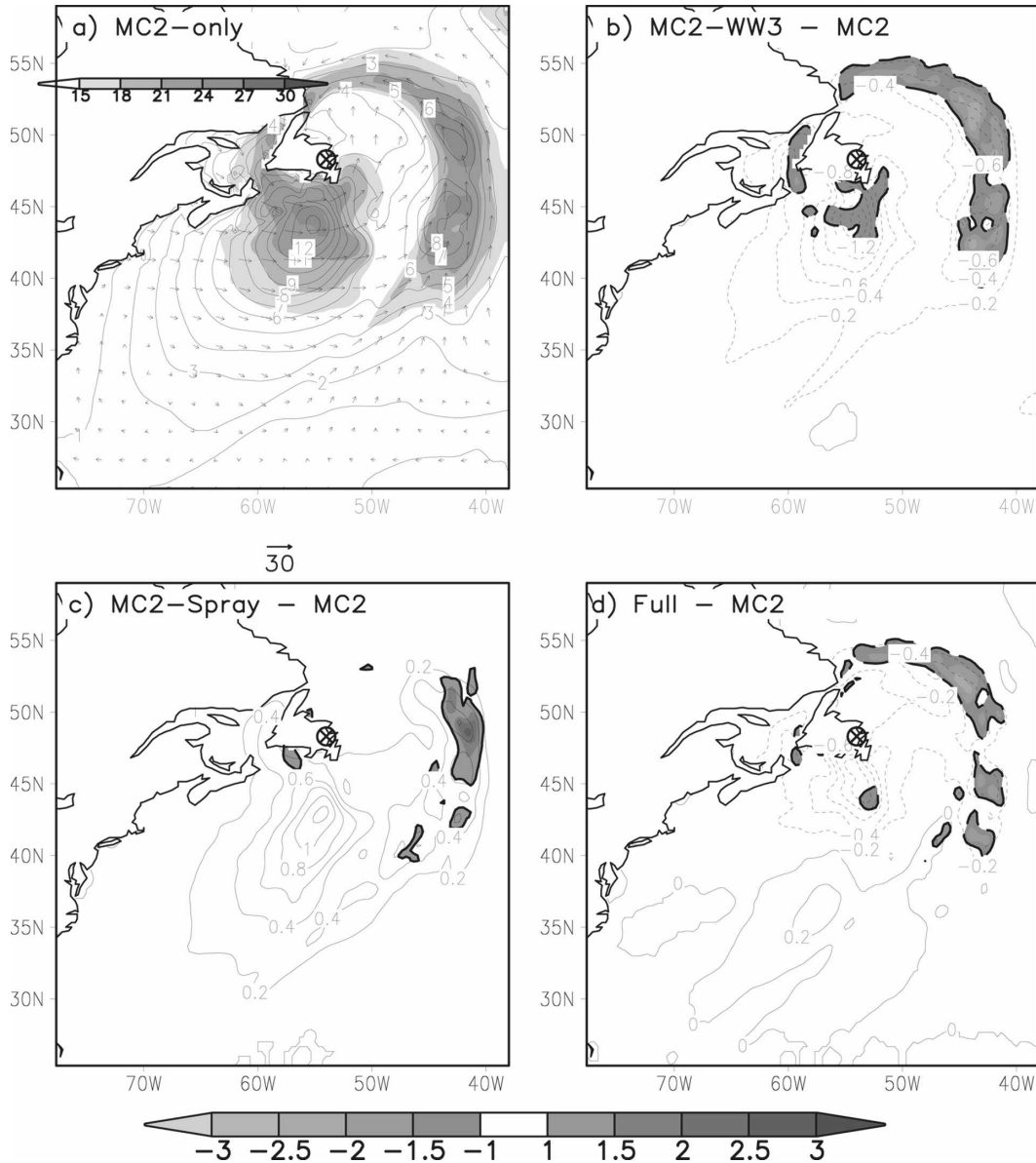


FIG. 11. Simulation results for the bomb at 1800 UTC 14 Jan 2002, showing (a) significant wave heights (contours) and U_{10} (shading) for MC2-only model results and (b) differences in significant wave heights (contours) and U_{10} differences (shading, negative differences contoured with black dashed lines and positive differences contoured with black solid lines) for MC2-wave minus MC2-only model results. (c) The same as (b), but for MC2-spray minus MC2-only model results. (d) The same as (b), but for fully coupled minus MC2-only model results. Storm centers are marked by a crossed circle.

superbomb in Figs. 14a–d, when their translational speeds are in the decelerating and accelerating stages, respectively (Fig. 10). These results show that the misalignment in rapidly moving asymmetric baroclinic storms can be quite different from Hurricane Bonnie, which was a slowly moving symmetric tropical storm, particularly in the high-wind regions around the storm center. A common feature in both the bomb and the superbomb is that there is a narrow transition belt to

the east and south of the storm center bounded roughly by the 15–20 m s^{-1} wind speed contour, where the dominant wave and wind directions are generally colinear. To the east of this transition belt, swell-dominated waves propagate to the right of the wind direction with increasing directional spread as the distance from the storm center increases. To the left of this transition belt, the dominant waves are generally to the left of the wind direction with increasing directional

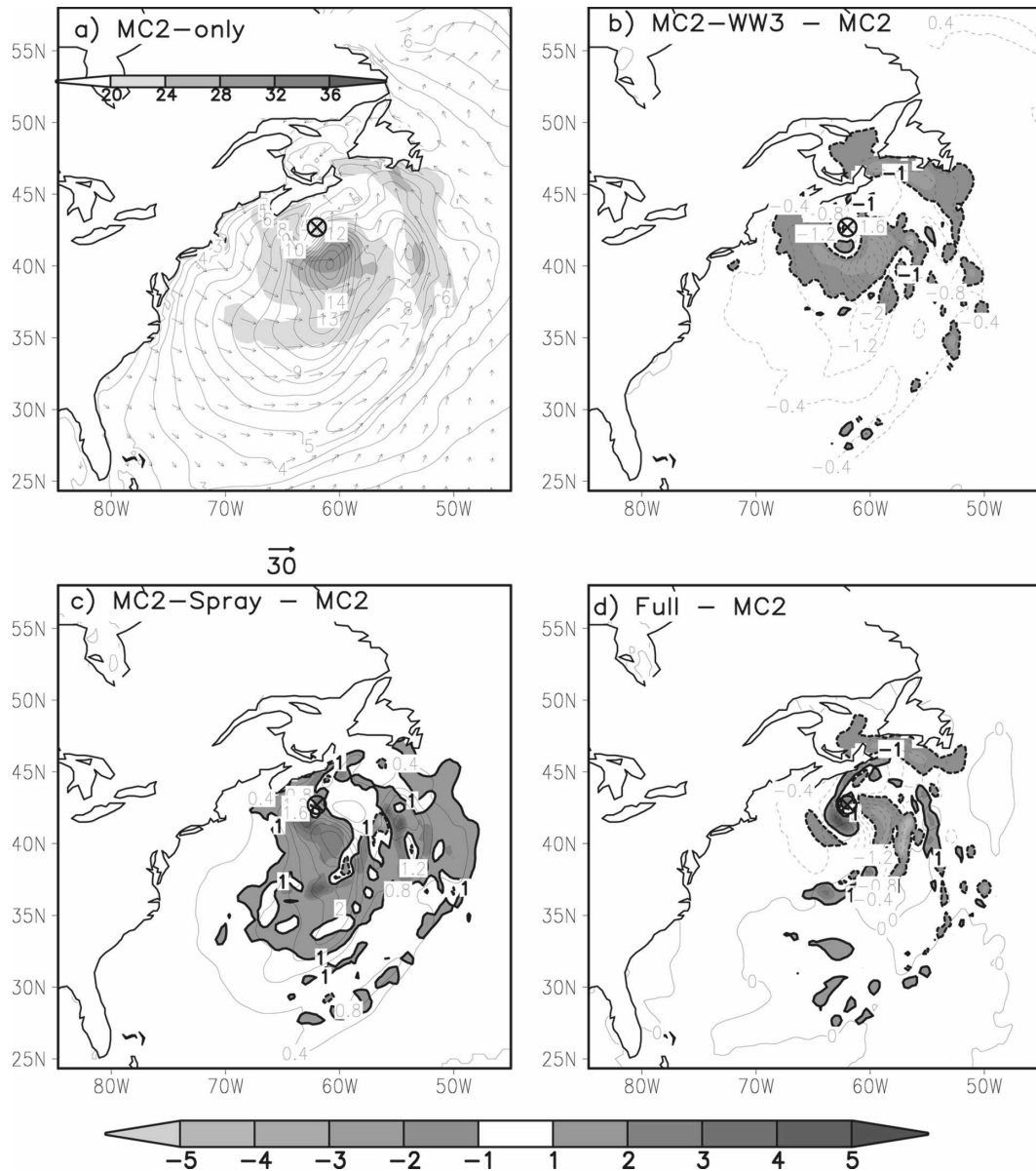


FIG. 12. As in Fig. 11, but for the superbomb at 1800 UTC 21 Jan 2000.

spread as the distance from the storm center decreases, which is a consequence of the curvature of storm-generated local wind fields and of the storm's translational motion. Moreover, Fig. 5 shows that the directions of both wind and dominant waves are not sensitive to spray and wave drag. Thus, spray and wave drag can increase or reduce the magnitude of wind depending on the competitive impact they exert, but they have no apparent influence on the dominant wave directions.

Moon et al. (2004) suggested that as the hurricane translation speed increases and waves become “trapped” within a hurricane, the dominant waves are mostly de-

termined by the swell produced by a resonance effect, and the swell waves propagate in the hurricane-track direction or to the left of the track. Therefore, in their simulations of Hurricane Bonnie, the maximum directional difference between wind and dominant waves is found in the hurricane's front left quadrant, especially in the rapidly moving stage. However, we found that the maximum misalignment is in the south and rear left quadrant of the bomb and the superbomb and that these two winter storms move much faster than do the dominant waves (Fig. 10). Thus, the waves are left behind and tend to occur in regions of lighter winds (Young 2003); the extent to which energy is pumped

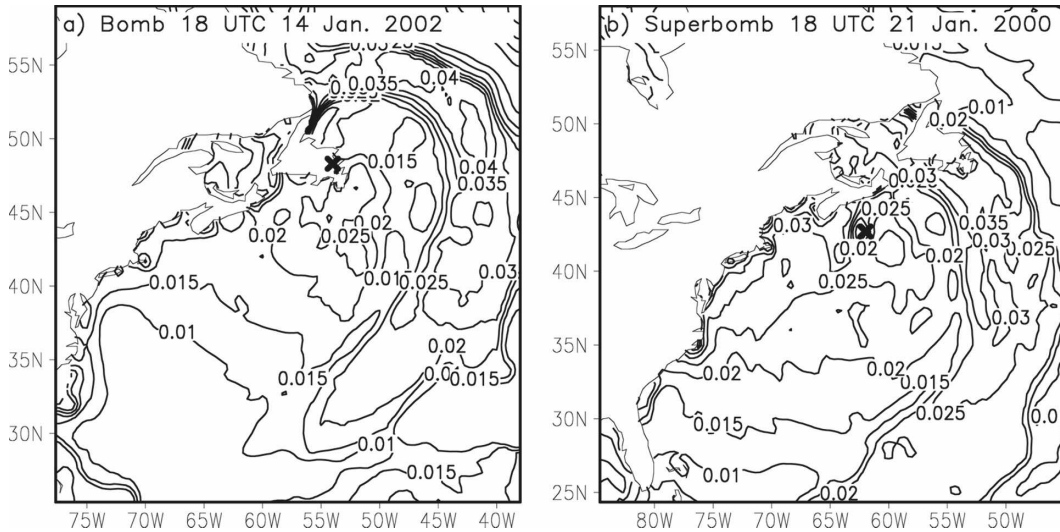


FIG. 13. Charnock parameter from MC2-wave simulation for (a) the bomb on 1800 UTC 14 Jan 2002 and for (b) the superbomb on 1800 UTC 21 Jan 2000. Storm centers are marked by an x.

from the atmosphere into the waves is limited, and the resonance effect does not play a dominant role.

To clarify the effect of translation speed, we performed an idealized experiment with a symmetric analytical Holland (1980) model to represent the storm winds associated with a tropical hurricane in a deep square-box ocean that is 1500 km (east–west) by 4000 km (north–south). The idealized hurricane is assumed to move north at a translation speed of 15 m s^{-1} from an initial location that is at the middle of the southern ocean boundary. Thus, the storm is able to outrun the dominant waves, which propagate at a group velocity of $\sim 10 \text{ m s}^{-1}$. In this experiment, the radius of maximum wind speed is set at 100 km, the centered and ambient pressures are 953 and 1012 mb, respectively, and the maximum wind speed is $\sim 45 \text{ m s}^{-1}$. The WW3 physics setup is the same as that used in the bomb and the superbomb simulations. After a spinup of 54 h, when a quasi-steady state is reached, the maximum directional difference between wind and dominant waves is found to the south of the radius of maximum wind (Fig. 14e), as in the bomb and the superbomb (Figs. 14a–d), because the waves are left behind the more rapidly moving storm. Thus, waves behind the radius of maximum wind are larger than waves in front of the radius of maximum wind. A transition belt, where the dominant wave and wind directions are generally collinear, also exists east of the radius of maximum wind. Left of this transition belt, the dominant waves propagate to the left of wind, behaving analogously to real storm cases. Elsewhere, dominant waves are found to the right of the wind direction.

e. Directional wave spectra related to storm translation speed

The spectrum produced by a storm is complex; factors include the spectrum's distance from the radius of maximum wind, locations from the storm center, and the storm translation speed (Moon et al. 2003). Given that WW3 has shown good capability to yield successful simulations of directional wave spectra (Moon et al. 2003; Doyle 2002; Tolman et al. 2002), we consider spectra from the coupled MC2-wave simulation at buoys 44141 and 44142 in this section.

For the bomb, we select three times—0600, 1200, and 1800 UTC 14 January 2002—when the translation speed of the bomb is accelerating (Fig. 10a). Although the distances from the buoys to the radius of maximum wind and the relative positions to the storm center are different, the directional wave spectra from the MC2 wave show a unimodal shape and the dominant waves propagate to the right of and almost parallel to the wind direction (Fig. 15). At these three times (0600, 1200, and 1800 UTC), buoy 44142 is ~ 200 km southwest, ~ 350 km west, and ~ 600 km west of the radius of maximum wind, while buoy 44141 is ~ 600 km southeast, ~ 100 km southeast of the radius of maximum wind, and within the radius of maximum wind (Figs. 16a–c), respectively. This occurs because the bomb moves much faster than the dominant waves (Fig. 10a); thus, there is less interaction between swell and wind sea, and the interaction between waves and the storm becomes decoupled because of the very rapid storm propagation speed.

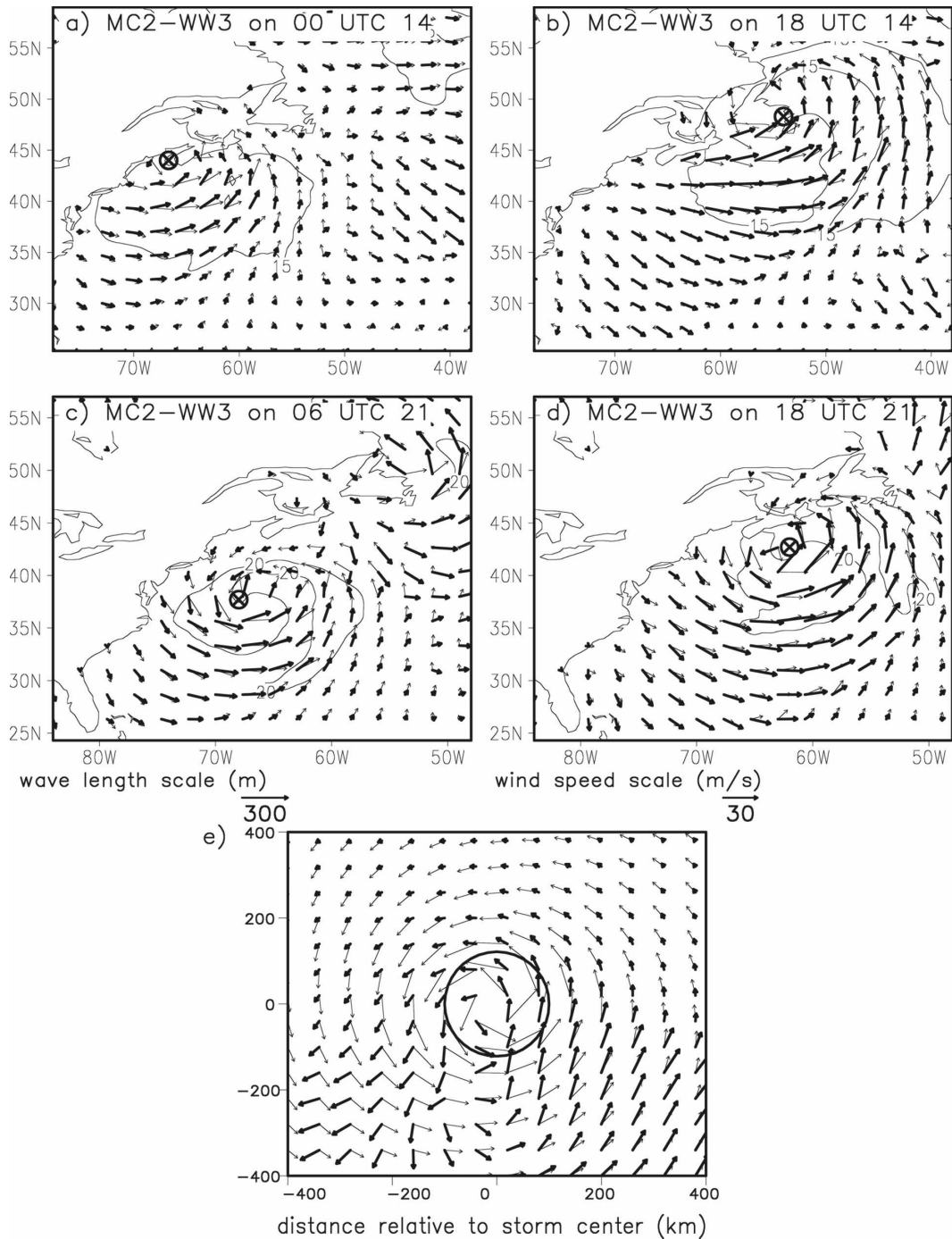


FIG. 14. Comparison of wind direction (light arrows) and dominant-wave direction (heavy arrows) from MC2-wave simulation for (a) 0000 and (b) 1800 UTC 14 Jan 2002 for the bomb and (c) 0600 and (d) 1800 UTC 21 Jan 2000 for the superbomb, showing 15 m s^{-1} wind speed contours in (a) and (b), and 20 m s^{-1} contours in (c) and (d). (e) The idealized experiment with a fixed translation speed of 15 m s^{-1} . The solid circle represents the radius of maximum wind.

For the superbomb, we select 1200 and 2100 UTC 21 January 2000, when the storm has a decelerating translation speed and the group speed of the dominant wave is comparable to the translation speed (Fig. 10b). At

1200 UTC 21 January 2000, the directional wave spectrum of buoy 44142 is unimodal (as shown in Fig. 17a). At this time, the buoy is just to the north of both the storm center and the radius of maximum wind

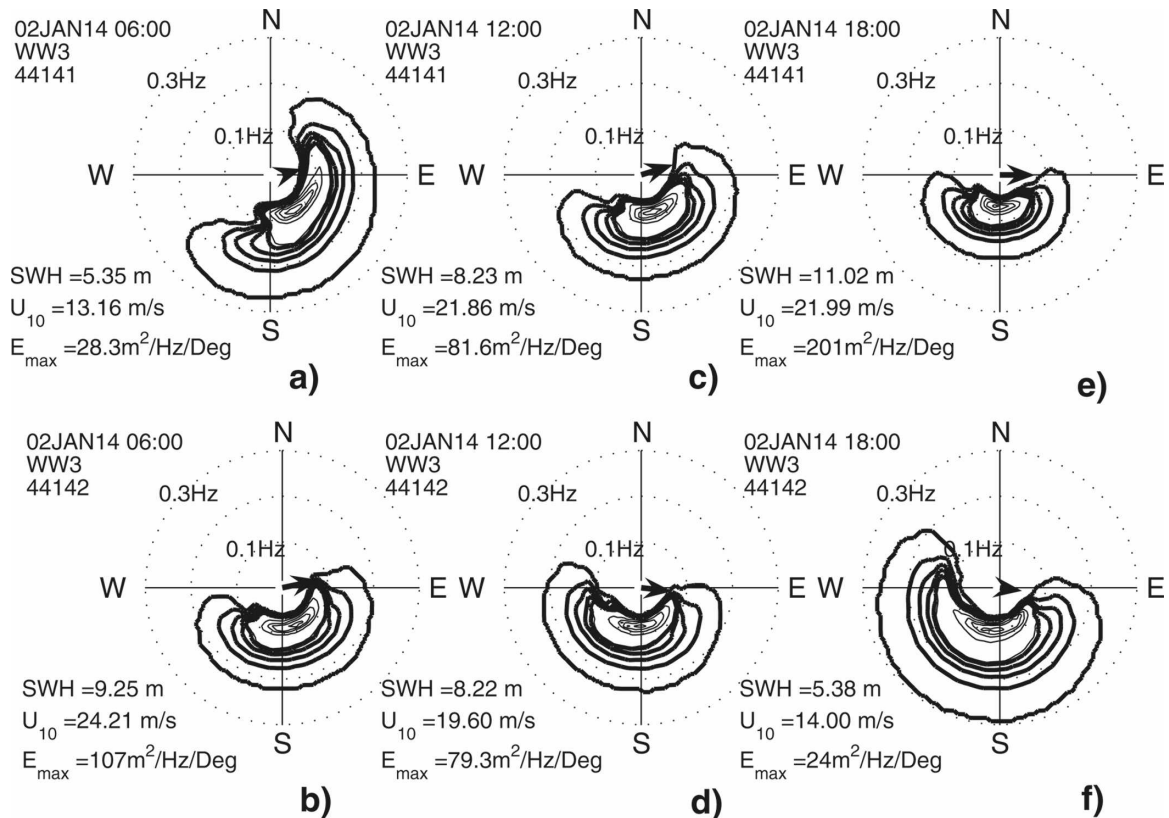


FIG. 15. Directional wave spectra from MC2-wave simulations at buoys 44141 and 44142. The dashed circles indicate the frequency (Hz). The spectrum is normalized with maximum energy and linearly spaced from 10%–90% at 20% intervals in thin lines, and 1%–9% with 2% intervals in thick lines. Values for SWHs, wind speed U_{10} , and the maximum peak spectral density E_{max} are shown. The thick arrows indicate the downwind direction with length proportional to wind speed. A wind speed of 30 m s^{-1} corresponds to a 0.1-Hz length of the contour radius.

(the latter is shown in Fig. 18a). By comparison, buoy 44141 is far from the storm center and the radius of maximum wind. However, when the largest wind field curvature is on the right forward quadrant (Fig. 18a), the directional spectra have a bimodal structure with higher wave energy to the left and lower wave energy to the right (Fig. 17b). At 2100 UTC 21 January 2000, buoy 44142 is ~ 350 km southwest of the storm center and ~ 300 km west of the radius of maximum wind (Fig. 18b), and the directional wave spectrum has a bimodal structure with high energy to the left and low energy to the right (Fig. 17c). However, at this time, buoy 44141 is far from the storm center and ~ 100 km east of the radius of maximum wind (Fig. 18b), and the resultant spectrum is unimodal (Fig. 17d).

Comparison of the observations and simulations in Moon et al. (2003) and Doyle (2002) suggests that to the rear and to the left of the storm track relative to the storm center, the directional wave spectra have more complex wave states because of the coexistence of wind waves and swell waves, while in the right forward quadrant of the hurricane eye, a unimodal propagating spec-

trum in the storm translation direction is more common. In retrospect, this kind of tendency occurs at buoy 44142 (Figs. 17a,c) during the superbomb, when it is to the north and ~ 300 km southwest of the storm center (Fig. 18b). The directional wave spectra at locations to the east, north, south, and west of the storm center (beyond the radius of maximum wind) produced by the idealized experiments mentioned in section 4d confirm this result.

Overall, directional wave spectra from MC2 spray tend to contain qualitatively similar structures to those contained in the MC2-wave simulation. The only difference is in the magnitude of the spectral density, which again suggests that including wave drag reduces wave height whereas including sea spray increases wave height. Neither wave drag nor sea spray affects the directional wave spectrum.

5. Conclusions

In this study, a coupled atmosphere–wave–sea spray model system is used to investigate the impacts of sea

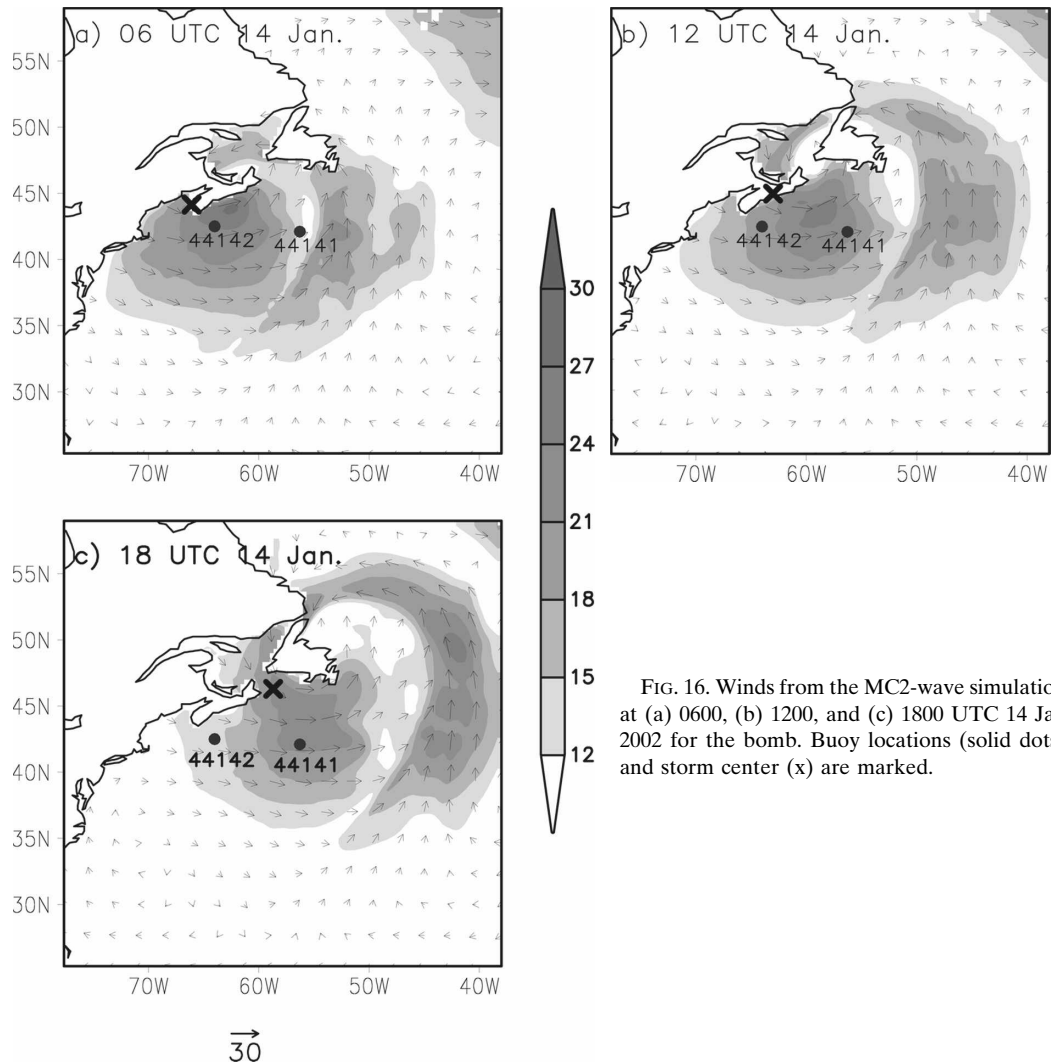


FIG. 16. Winds from the MC2-wave simulation at (a) 0600, (b) 1200, and (c) 1800 UTC 14 Jan 2002 for the bomb. Buoy locations (solid dots) and storm center (x) are marked.

spray and wave drag on storm-generated waves with respect to the storm location and translation speed. Two rapidly moving intense winter storms, the bomb from January 2002 and the superbomb from January 2000, are considered. Zhang et al. (2006) present detailed considerations regarding the mechanisms by which surface fluxes affect storm intensification or deintensification. They found that when wind speeds are high and sea surface temperatures (SSTs) are warm, spray can significantly increase the surface heat fluxes. On the other hand, whereas momentum fluxes related to wave drag are important over regions of the storm where young, newly generated waves are prevalent (e.g., during the rapid-development phase of the storm), their effect decreases where the waves reach maturity. Zhang et al. (2006) found that the collective influence of spray and waves on storm intensity depends on their occurrence in the early stages of a

storm's rapid-intensification phase and on their spatial distribution with respect to the storm center. A potential vorticity framework can be used to show the relative importance of these surface fluxes' impacts compared to baroclinic processes.

In this present study, results show that the decrease or increase of significant wave heights due to wave drag and spray effects is most significant in high-wind regions to the right of the storm track. This occurs despite the complexity of the sea state in regions of strong directional wind field curvature. Because the storm translation speed exceeds the propagation speed of the dominant waves, particularly when the storm moves in the same direction as the local wind, maximum wave heights tend to appear several hours after the peak wind events.

Because the combined influences of spray and wave are competitive with each other, the final significant

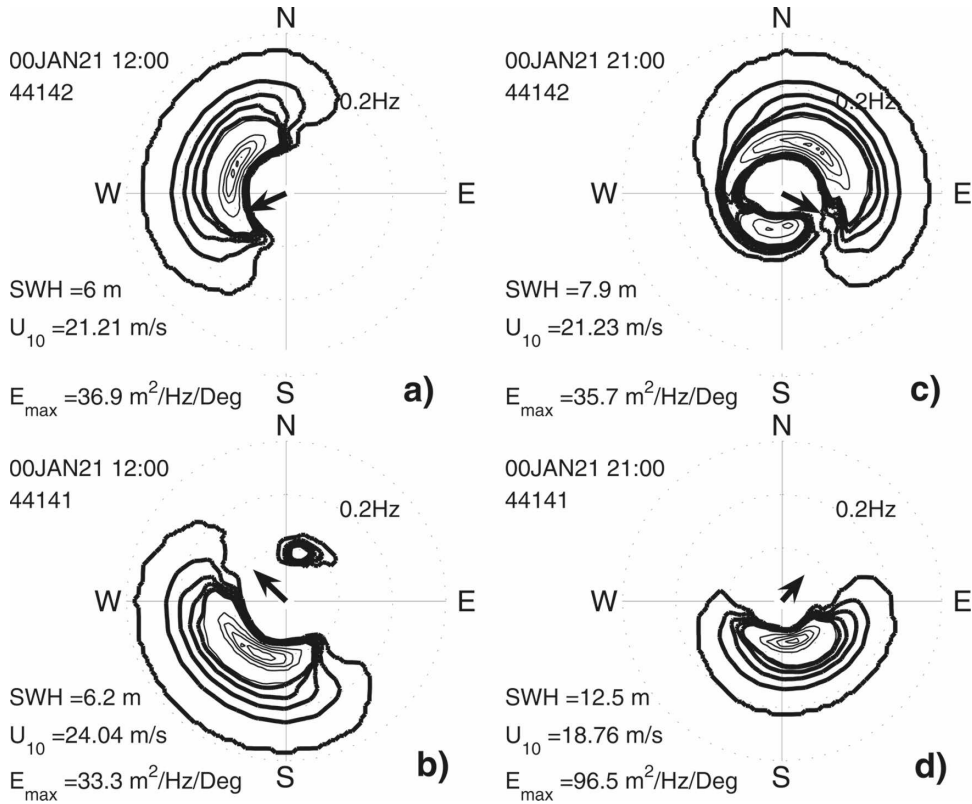


FIG. 17. As in Fig. 15, but for the superbomb.

wave heights can be close to the significant wave heights from the uncoupled MC2-only runs. This result is obtained in the case of the superbomb; the increase in significant wave height due to spray is comparable with

the decrease due to wave drag, and the combined influence of both processes is close to the observed significant wave height values. Results from the bomb are less clear; a full understanding of the dynamical system

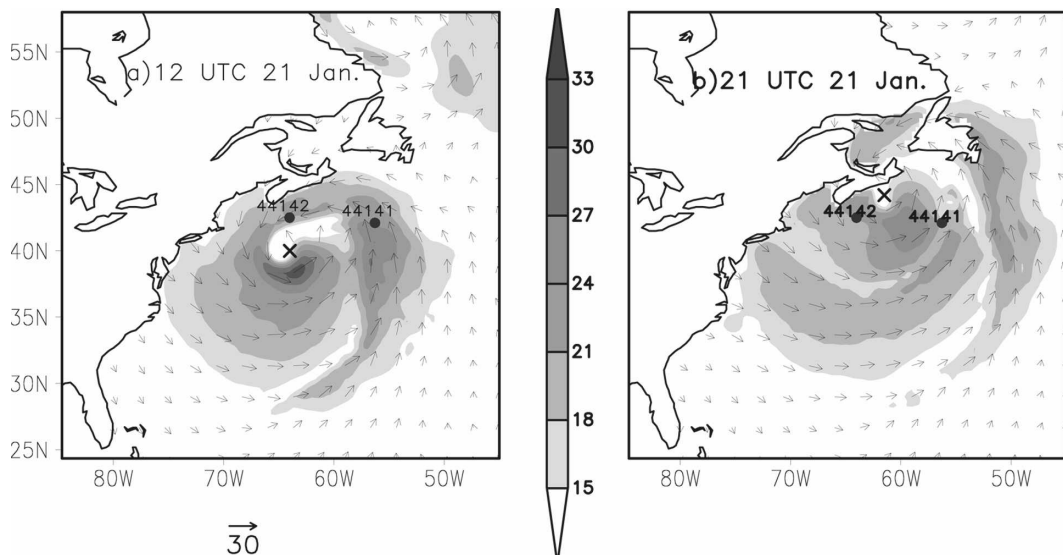


FIG. 18. Winds from the MC2-wave simulation at (a) 1200 and (b) 2100 UTC 21 Jan 2000.

is constrained by the uncertainty in our quantitative parameterizations for wave–spray processes.

Refinements in the upper limit of the Z_{0m} or its variation for winds in the range of $U_{10} < 30 \text{ m s}^{-1}$ will not change our general conclusions that the effects of spray and waves compete in terms of their impacts on storm intensity and wave development. Modification of parameterizations for Z_{0m} or sea spray would change the magnitude of the competition. The relative importance of wave drag, as compared to sea spray contributions, was estimated for the two storms considered in this study (Figs. 11, 12). In the cases considered, wave drag may de-intensify winds (U_{10}) by as much as about $2\text{--}3 \text{ m s}^{-1}$ or 10%, sea spray may intensify winds by about $2\text{--}5 \text{ m s}^{-1}$, or 10%–20%. However, at the peak of the storms, the net contribution is not simply a cancellation of contributions but can vary by about 10%–15% throughout the distribution of the storm structure. By comparison, synoptic variability, in terms of an ensemble of storm simulations, is on the order of 0.5 to 1 m s^{-1} , or about 5%–10%.

In the open ocean, the dominant waves associated with hurricanes with increasing translational speed may mostly be determined by the swell produced by the resonance, whereby storm propagation speed coincides with the dominant wave speed. These waves are propagating along the hurricane track direction or to the left of the track. In this study, the two storms move faster than the dominant waves, implying that wave trapping (or resonance) is not dominant because waves are left behind the more rapidly moving storms. Our real and idealized storm simulations show that a transition belt exists east of the radius of maximum wind, where the dominant wave and wind directions are generally colinear. Left of this transition belt, the dominant waves propagate to the left of the wind direction. Elsewhere, dominant waves are found to the right of the wind direction. We show that the directions of both wind and dominant waves are not sensitive to our formulations of spray and wave drag and that although these processes can increase or reduce the wind speed, they have no apparent effect on the directional spectrum.

The spatial variation of the directional wave spectra is dependent on the relative position of the storm center and the storm translation speed. During rapidly accelerating translation storm speeds, the storm can move much faster than the dominant waves and leave them behind. Thus, there is less interaction between swell and wind sea and the storm tends to decouple from the ocean surface. The resulting directional wave spectra tend to have a relatively simple unimodal structure. During the decelerating translation storm speeds, the group speed of the dominant waves converges to the

storm translational speed. The directional wave spectra tend to be more complicated than those occurring when the storm accelerates ahead of the waves. Moreover, the directional wave spectra *behind* a rapidly moving storm generally have a more complex wave structure because of wave interactions with swell, whereas ahead of a slowly moving storm, spectra tend to have a unimodal structure propagating in the direction of the hurricane.

Acknowledgments. The authors want to acknowledge the painstaking efforts of two reviewers who have helped us to greatly improve the manuscript. Support is from the Canadian Panel on Energy Research and Development (Offshore Environmental Factors Program), ONR (U.S. Office of Naval Research) via the Gulf of Maine Ocean Observing System (GoMOOS), the Southeast Universities Research Association Coastal Ocean Observing and Prediction (SCOOP) program, and the Canada Foundation for Climate and Atmospheric Studies (CFCAS).

REFERENCES

- Andreas, E. L., 1992: Sea spray and the turbulent air–sea heat fluxes. *J. Geophys. Res.*, **97**, 11 429–11 441.
- , 1995: The temperature of evaporating sea spray droplets. *J. Atmos. Sci.*, **52**, 852–862.
- , 1998: A new sea spray generation function for wind speeds up to 32 m s^{-1} . *J. Phys. Oceanogr.*, **28**, 2175–2184.
- , 2003: An algorithm to predict the turbulent air–sea fluxes in high-wind spray conditions. Preprints, *12th Conf. on Interaction of the Sea and Atmosphere*, Long Beach, CA, Amer. Meteor. Soc., 3.4.
- , and J. DeCosmo, 1999: Sea spray production and influence on air–sea heat and moisture fluxes over the open ocean. *Air–Sea Exchange: Physics, Chemistry and Dynamics*, G. L. Geernaert, Ed., Kluwer, 327–362.
- , and K. A. Emanuel, 2001: Effects of sea spray on tropical cyclone intensity. *J. Atmos. Sci.*, **58**, 3741–3751.
- , and J. DeCosmo, 2002: The signature of sea spray in the HEXOS turbulent heat flux data. *Bound.-Layer Meteor.*, **103**, 303–333.
- Benoit, R., M. Desgagne, P. Pellerin, S. Pellerin, Y. Chartier, and S. Desjardins, 1997: The Canadian MC2: A semi-Lagrangian, semi-implicit wideband atmospheric model suited for fine-scale process studies and simulation. *Mon. Wea. Rev.*, **125**, 2382–2415.
- Bowyer, P., and A. MacAfee, 2005: The theory of trapped-fetch waves with tropical cyclones—An operational perspective. *Wea. Forecasting*, **20**, 229–244.
- Charnock, H., 1955: Wind stress on a water surface. *Quart. J. Roy. Meteor. Soc.*, **81**, 639–640.
- Desjardins, S., J. Mailhot, and R. Lalbeharry, 2000: Examination of the impact of a coupled atmospheric and ocean wave system. Part I: Atmospheric aspects. *J. Phys. Oceanogr.*, **30**, 385–401.
- Donelan, M. A., B. K. Haus, N. Reul, W. J. Plant, M. Stiassnie, H. C. Graber, O. B. Brown, and E. S. Saltzman, 2004: On the

- limiting aerodynamic roughness of the ocean in very strong winds. *Geophys. Res. Lett.*, **31**, L18306, doi:10.1029/2004GL019460.
- Doyle, J. D., 1995: Coupled ocean wave/atmosphere mesoscale model simulations of cyclogenesis. *Tellus*, **47A**, 766–778.
- , 2002: Coupled atmosphere–ocean wave simulations under high wind conditions. *Mon. Wea. Rev.*, **130**, 3087–3099.
- Drennan, W. M., 2006: On parameterisations of air–sea fluxes. *Atmosphere–Ocean Interactions*, W. Perrie, Ed., Vol. 2, WIT Press, 1–34.
- , H. C. Graber, D. Hauser, and C. Quentin, 2003: On the wave age dependence of wind stress over pure wind seas. *J. Geophys. Res.*, **108**, 8062, doi:10.1029/2000JC000715.
- Emanuel, K. A., 1995: Sensitivity of tropical cyclones to surface exchange coefficients and a revised steady-state model incorporating eye dynamics. *J. Atmos. Sci.*, **52**, 3969–3976.
- , 2003: A similarity hypothesis for air–sea exchange at extreme wind speeds. *J. Atmos. Sci.*, **60**, 1420–1428.
- Fairall, C. W., J. D. Kepert, and G. J. Holland, 1994: The effect of sea spray on surface energy transports over the ocean. *Global Atmos. Ocean Syst.*, **2**, 121–142.
- , E. F. Bradley, D. P. Rogers, J. B. Edson, and G. S. Young, 1996: Bulk parameterization of air–sea fluxes for Tropical Ocean–Global Atmosphere Coupled–Ocean Atmosphere Response Experiment. *J. Geophys. Res.*, **101**, 3747–3764.
- Holland, G. J., 1980: An analytical model of the wind and pressure profiles in hurricanes. *Mon. Wea. Rev.*, **108**, 1212–1218.
- Janssen, P. A. E. M., 1991: Quasi-linear theory of wind-wave generation applied to wave forecasting. *J. Phys. Oceanogr.*, **21**, 1631–1642.
- , J. D. Doyle, J. Bidlot, B. Hansen, L. Isaksen, and P. Viterbo, 2002: Impact and feedback of ocean waves on the atmosphere. *Atmosphere–Ocean Interactions*, W. Perrie, Ed., Vol. 1, WIT Press, 155–197.
- Kain, J. S., and J. M. Fritsch, 1993: Convective parameterization for mesoscale models: The Kain–Fritsch scheme. *The Representation of Cumulus Convection in Numerical Models, Meteor. Monogr.*, No. 46, Amer. Meteor. Soc., 165–170.
- Komen, G. J., L. Cavaleri, M. Donelan, K. Hasselmann, S. Hasselmann, and P. A. E. M. Janssen, 1994: *Dynamics and Modeling of Ocean Waves*. Cambridge University Press, 532 pp.
- Lalbeharry, R., J. Mailhot, S. Desjardins, and L. Wilson, 2000: Examination of the impact of a coupled atmospheric and ocean wave system. Part II: Ocean wave aspects. *J. Phys. Oceanogr.*, **30**, 402–415.
- Large, W. G., and S. Pond, 1981: Open ocean momentum flux measurements in moderate to strong wind. *J. Phys. Oceanogr.*, **11**, 324–336.
- Lionello, P., P. Malguzzi, and A. Buzzi, 1998: Coupling between the atmospheric circulation and the ocean wave field: An idealized case. *J. Phys. Oceanogr.*, **28**, 161–177.
- Liu, W. T., K. B. Katsaros, and J. A. Businger, 1979: Bulk parameterization of air–sea exchanges of heat and water vapor including the molecular constraints at the interface. *J. Atmos. Sci.*, **36**, 1722–1735.
- McTaggart-Cowan, R., J. R. Gyakum, and M. K. Yau, 2001: Sensitivity testing of extratropical transitions using potential vorticity inversions to modify initial conditions: Hurricane Earl case study. *Mon. Wea. Rev.*, **129**, 1617–1636.
- Moon, I.-J., I. Ginis, T. Hara, H. Tolman, C. W. Wright, and E. Walsh, 2003: Numerical simulation of sea surface directional wave spectra under hurricane wind forcing. *J. Phys. Oceanogr.*, **33**, 1680–1706.
- , —, and —, 2004: Effect of surface waves on air–sea momentum exchange. Part II: Behavior of drag coefficient under tropical cyclones. *J. Atmos. Sci.*, **61**, 2334–2348.
- Perrie, W., E. L. Andreas, W. Zhang, W. Li, J. Gyakum, and R. McTaggart-Cowan, 2005: Sea spray impacts on intensifying midlatitude cyclones. *J. Atmos. Sci.*, **62**, 1867–1883.
- Powell, M. D., P. J. Vickery, and T. A. Reinhold, 2003: Reduced drag coefficient for high wind speeds in tropical cyclones. *Nature*, **422**, 279–283.
- Smith, S., and Coauthors, 1992: Sea surface wind stress and drag coefficient: The HEXOS results. *Bound.-Layer Meteor.*, **60**, 109–142.
- Tolman, H. L., and D. Chalikov, 1996: Source terms in a third-generation wind wave model. *J. Phys. Oceanogr.*, **26**, 2497–2518.
- , B. Balasubramanian, L. D. Burroughs, D. Chalikov, Y. Y. Chao, H. S. Chen, and V. M. Gerald, 2002: Development and implementation of wind-generated ocean surface wave models at NCEP. *Wea. Forecasting*, **17**, 311–333.
- Walsh, E. J., and Coauthors, 2002: Hurricane directional wave spectrum spatial variation at landfall. *J. Phys. Oceanogr.*, **32**, 1667–1684.
- Wang, Y., J. D. Kepert, and G. J. Holland, 2001: The effect of sea spray evaporation on tropical cyclone boundary layer structure and intensity. *Mon. Wea. Rev.*, **129**, 2481–2500.
- Young, I. R., 2003: A review of the sea state generated by hurricanes. *Mar. Struct.*, **16**, 201–218.
- Zhang, Y., and W. Perrie, 2001: Feedback mechanisms for the atmosphere and ocean surface. *Bound.-Layer Meteor.*, **100**, 321–348.
- , —, and W. Li, 2006: Impacts of waves and sea spray on midlatitude storm structure and intensity. *Mon. Wea. Rev.*, **134**, 2418–2442.